Hybrid approaches coupling sol–gel and plasma for the deposition of oxide-based nanocomposite thin films: a review

Maria Mitronika, Agnès Granier, Antoine Goullet, Mireille Richard-Plouet

▶ **To cite this version:**

Maria Mitronika, Agnès Granier, Antoine Goullet, Mireille Richard-Plouet. Hybrid approaches coupling sol–gel and plasma for the deposition of oxide-based nanocomposite thin films: a review. SN Applied Sciences, 2021, 3 (6), pp.665. ⟨10.1007/s42452-021-04642-0⟩. ⟨hal-03386299⟩

HAL Id: hal-03386299

https://hal.science/hal-03386299v1

Submitted on 25 Oct 2021

HAL is a multi-disciplinary open access archive for the deposit and dissemination of scientific research documents, whether they are published or not. The documents may come from teaching and research institutions in France or abroad, or from public or private research centers.

L'archive ouverte pluridisciplinaire **HAL**, est destinée au dépôt et à la diffusion de documents scientifiques de niveau recherche, publiés ou non, émanant des établissements d'enseignement et de recherche français ou étrangers, des laboratoires publics ou privés.

HAL Authorization

Hybrid Approaches coupling sol-gel and plasma for the deposition of oxide-based nanocomposite thin films: A review

M. Mitronika[1], Agnès Granier[1], A. Goullet[1] and Mireille Richard-Plouet[1]

[1] *Université de Nantes, CNRS, Institut des Matériaux Jean Rouxel, IMN, F-44000 Nantes, France*

ORCID iDs
Maria Mitronika https://orcid.org/0000-0002-2918-2579
Agnès Granier https://orcid.org/0000-0002-1054-8139
Antoine Goullet https://orcid.org/0000-0001-5411-4351
Mireille Richard-Plouet https://orcid.org/0000-0002-7871-2919

Abstract: In view of developing new materials with enhanced properties, such as nanocomposite (NC) thin films, special interest has been given in optimizing the deposition processes themselves. The latter, if well selected, could give the freedom to control the NCs synthesis and final properties. Attempting to overcome severe challenges observed when creating NC or oxide-based NC film, hybrid approaches combining injection of colloidal solutions and plasma processes have been proposed. This review focuses on oxide based NCs, using as an example the TiO_2 NPs and SiO_2 matrix as NCs, while investigating their optical and dielectric properties. Additionally, this review presents the state-of-the-art in processes for the preparation of the NCs. The major categories of hybrid approaches coupling sol-gel and plasma processes are given. Finally, a comparative study among the published works is provided, aiming in highlighting the impact that each approach has on the physical and chemical characteristics of the produced NCs.

Keywords: oxides, TiO_2, SiO_2, nanocomposite, thin film, deposition processes, hybrid approaches

1. Introduction

Nanocomposites and nanostructured materials have gained the attention, as the properties of the resulting composite are likely to differ from the original bulk ones. [1] They are part of a more general category, the one of Nanomaterials (NMs). Nanomaterial (NM) is defined as the "material with any external

dimension in the nanoscale or having internal structure or surface structure in the nanoscale", with nanoscale defined as the "length range approximately from 1 nm to 100 nm" (ISO/TS 80004-1:2015.

Nanocomposites are solid materials composed of at least two phases among which one exhibits nanoscale dimensions.[2,1,3] The definition of phase refers here to a medium for which no abrupt change in composition or density is observed. The surface-to-volume ratio due to the nanometric objects is very high, and their behaviour becomes controlled by surface properties rather than by volume properties. In addition to this, the interactions between the interfaces of the phases become more important in terms of dimension and for the resulting property. Consequently, the materials can have novel chemical and physical properties that depend on the morphology and interfacial characteristics of the component materials. Since 1996 and based on a search in Web of Science using the keywords TiO_2, SiO_2 and NCs (carried out 12th of June 2020), nanocomposites have been an emerging field providing in an exponential rate many scientific works, reaching in 2019 a total amount of 15.790 records. Their applications are rather broad with some of the most predominant ones being the packaging, insulations, antimicrobial, antireflective, self-cleaning, solar cells, sensors, and optics. [4–9]

Due to the versatile configuration these two phase materials can have, some works focused in their theoretical study, using effective medium theories (EMT) [10,11], Volume Averaging Theory(VAT) [12]or the Lippmann-Schwinger equation [13]. Garahan et al. used the VAT model and finite elements to describe the boundary conditions of the nano-inclusion shapes, for the effective dielectric (κ) and electrical properties and derived the effective index of refraction n_{eff} and absorption index k_{eff} of nanoporous materials. These results were used to predict the behavior of the optical properties of nanocomposite materials. It was found out that due to the presence of strongly absorbing dispersed phase such as metallic nanowires, the effective refractive index was much smaller than each of the two continuous or dispersed phases. Rao et al. [10], while comparing different EMTs for polymer-based NCs (TiO_2 NPs, polymer matrix) stressed out that the use of the effective medium can hold only when the two phases are chemically independent (no chemical binding between the components). In addition, Lozovski et al. [13] indicated that the size of the nanoparticles or more generally the filler, the thickness of the nanocomposite and the distance the filler is located from the substrate can play a key role in the optical absorption of the NC. The aim of these studies was to render it possible through this theoretical analysis to predict the properties of the final NCs, even if they were not implemented and characterized experimentally. In detail, it is proposed that knowing the tuneable parameters that could affect the optical response (such as the filling factor, the nature

of the NPs and matrix, the size and shape of the filler, the thickness of the NC, etc) can provide the guidelines for the design of the NCs oriented for the targeted applications. Also, the way (linear, parabolic etc) that the optical response is managed could additionally provide such guidelines.

In this work, a review on the hybrid processes coupling sol gel and plasma deposition techniques for the production of NC thin films is attempted. Initially, this review focuses on the interest oxide-based NCs can have, using as an example the TiO_2 NPs and SiO_2 matrix. Subsequently, the major categories of hybrid approaches coupling sol-gel and plasma processes are given. Finally, a comparative study is provided, aiming in highlighting the impact that each approach has on the physical and chemical characteristics of the produced NCs.

2 Oxide-based NC thin films: TiO_2 NPs and SiO_2 matrix

In general, nanoparticles can be classified depending on their nature (for example, carbon-based, ceramic, metallic, polymeric and semiconductor NPs [14]), size, morphology, physical and chemical characteristics, etc. Among the different existing dielectric materials, TiO_2, as high-κ (dielectric constant > 80 [8-9]), stable and low cost semiconductor has been identified as an ideal candidate for its optical [17], dielectric [8-9] and photocatalytic [18] properties. Trying to expand these properties, TiO_2 NPs were extensively prepared in different configurations [19] and studied especially for cosmetic [20], antibacterial [21], solar cell [22–25], self-cleaning [26], hydrophobic [27] and dielectric-isolative [28] applications. Given the different properties that the nanoparticles can have compared to the bulk materials, we gathered in this paragraph the effect of nanostructuration on the opto-electronic properties: band-gap, dielectric constant, optical index… and how they can be adjusted by preparing NC.

It is well-known and often observed experimentally that when the diameter of the crystallite of a semiconductor (SC) particle falls below a critical radius of about 10 nm, charge carrier behave quantum mechanically. As a result of this quantum confinement, as shown in Figure 1a). , the electron density of states of nanometric SC materials exhibits features which are intermediate between the situation of clusters, composed of discrete energy levels, and the one of periodic crystalline solids. Thus the electron structure is composed of wide bands, namely the valence (VB) and conduction bands (CB) separated by the band gap. The quantum confinement in nanocrystalline SC induces a narrowing of VB and CB and consequently this leads to the enlargement of the band gap . Those shifts of the band edges also introduce a modification of

the redox potentials associated to these levels. [29,30] Enright et Fitzmaurice [31] predicted the size dependence for the energy of the valence and conduction bands, which is given in Figure 1b. Based on this, for anatase nanocrystallites below 10 nm, a decrease in the band gap is observed. This decrease is more pronounced for nanocrystallite sizes below ~5 nm. Above the value of 10 nm, the band gap is expected to have similar behavior as the bulk material. A sensitive tool to follow the anatase nanocrystallite sizes is Raman spectroscopy and attempts to correlate the size of the TiO_2 crystallite with the Raman shift was carried out by Pighini et al. [32].

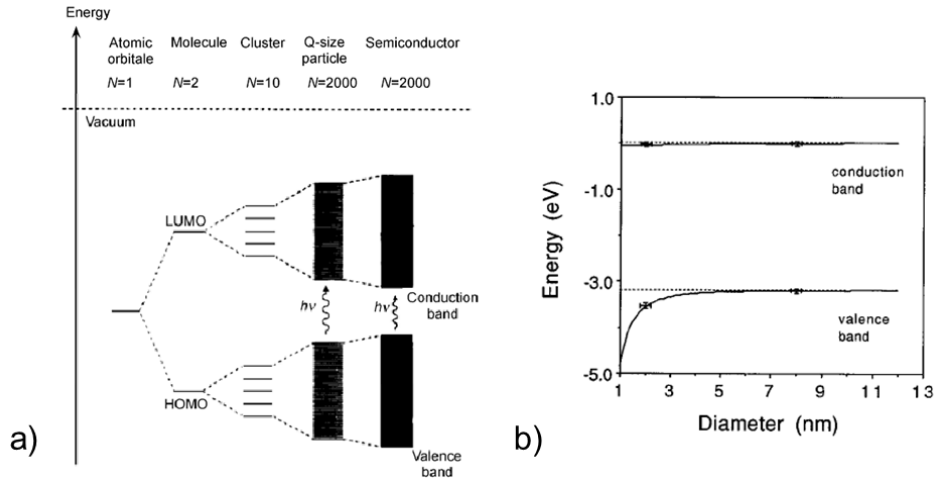

Figure 1: a) Molecular orbital (MO) model for particle growth of N monomeric units. The spacing of the energy levels (i.e., density of states) varies among systems. Reproduced with permission from [29], copyright 1995 ACS Publications. On the left-hand side of the scheme the bands of Q-size particles become narrower compared to the bulk semiconductor. b) Theoretical prediction of the Eg bandgap as a function of the particle radius. With bars, the experimentally determined changes in the energy of the valence and conduction band edges are plotted. Reproduced with permission from [31], copyright 1996 ACS Publications.

Regarding the dielectric characteristics TiO_2 NPs can have, in comparison to bulk materials or different NPs diameter, the work of Zhang et al. [33] was one of the earliest reports. As shown in Figure 2, the real part of the dielectric constant ε_r' was measured in a frequency range of 10^1 to 10^5 Hz.

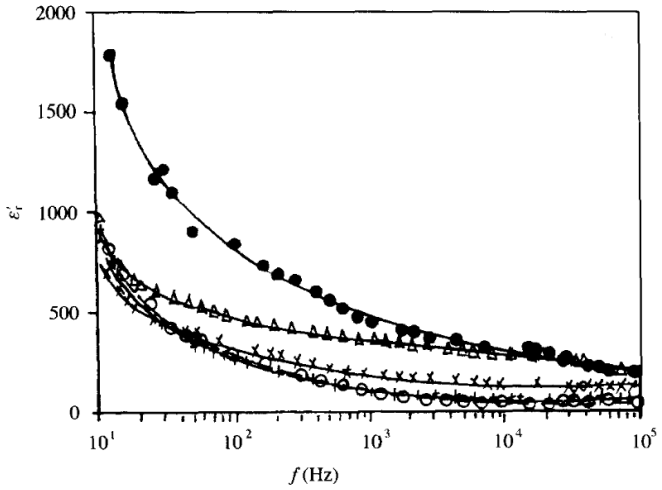

Figure 2: Spectra of dielectric constant as a function of the frequency f at room temperature for nano-TiO_2 with various particle diameters d. Anatase: (o) d = 9.8 nm, (Δ)14.4 nm, (.) 17.8 nm, (x) 28.5 nm, (+) coarse grains (~1 μm). Reproduced with permission from [33], copyright 2006 John Wiley and Sons Publishing.

Different size of anatase nanoparticles were used and were compared with TiO_2 anatase coarse grains with a size of ~1μm. The results indicated that in this frequency range, the dielectric constants of TiO_2 NPs have equal or larger values than the coarse grain anatase TiO_2. In addition to this, for larger diameter size (in the nanometre range) a higher value is observed especially in the low frequencies. In this frequency range, this effect originates from the polarization of the dielectric materials based on interfacial and space charge mechanisms. Hence, under the action of an external electric field, positive and negative space charges in the interfaces move towards negative and positive poles of the electric field, respectively. As a consequence, for coarse-grain TiO_2 NPs (large domains), the number of interfaces is very small and the space charge polarization becomes too weak to have an impact. Contrary to this, for small nanoparticles (nanometre range), the volume fraction of interfaces is much larger, so that the contribution of space charge polarization in interfaces to ε_r' becomes large enough to enhance the dielectric constant. These findings were later verified by other authors [34–36]. Specifically, it was observed that for several materials such as Aluminium Oxide, Titanium Oxide and Silicon Dioxide, the relative dielectric constant is 10 times higher for the nanoparticles in powder compacts than for the bulk materials [36].

Conventional dielectric materials are ceramics with large dielectric permittivity, coupled with high stiffness and excellent thermal stability. However, their applicability for passive components such as capacitors is largely impeded by their small breakdown strength and challenging processing conditions. Observing that these materials can exhibit enhanced characteristics in the nanoscale, attempts were carried

out to disperse them as fillers in matrix materials. The aim was to capitalize the high permittivity of such nanoparticles with the good electrical strength of the matrix resulting in the creation of nanocomposites with novel properties. Many works use polymer matrices as they exhibit high electrical strength, flexibility and can be easily processed. [37]. The drawback of these polymer matrices is that they lack in transparency or in high mechanical strength. Therefore, inorganic matrixes such as silica are a good alternative as they can exhibit significant isolative properties (high electrical strength), high mechanical strength and optical properties such as transparency in a broad spectral range.

Since 2014, approximately 892 publications including the keywords of TiO_2, SiO_2 and nanocomposites have been reported. The most cited applications of these works are regarding photocatalytic and antibacterial or dielectric and optical applications. Focusing mainly on the TiO_2-SiO_2 nanocomposites (TiO_2 NPs, SiO_2 matrix), Sarkar et al. [38] attempted to investigate the TiO_2-SiO_2 nanocomposite thin films elaborated by sol-gel. In this specific work, the size of the nanoparticles was varied from ~1 to 22 nm. At the same time for the larger NPs, a higher concentration of the Ti content was successfully achieved. Current density-electric field (J-E) measurements showed that for all the NPs sizes an ohmic conduction is observed in the low field. However, depending on the size of the TiO_2 NPs, their low field resistivity was found to decrease by a factor of 10^2 (from 2.2 10^{12} to 2.2 10^{10} Ω cm) for the larger sizes. The explanation given by the authors was that in these cases a percolated network of TiO_2 nanoparticles is created, controlling its conductivity. For higher electrical fields, as expected all compositions exhibit space-charge limited behaviour. For the nanocomposite with NPs sizes as low as ~1 nm, some oscillations were observed and this phenomenon was attributed to the single electron tunnelling effect (SET) caused by the small nanocrystallites isolated inside the amorphous silica matrix having a wide bandgap.

In recent years apart from studying the electrical response of such nanocomposites, nanoparticles have also been used to make transparent nanocomposite structures having high refractive indices. If the NPs are small compared to the wavelength of light, scattering is avoided, and the nanocomposites are transparent even at high nanoparticle filling factors. Hence, it is possible for the refractive index to be tuned over a wide range by changing the filling factor and type of filler. [12,39,40] Following this direction, Kermadi et al, examined the optical characteristics of sol-gel derived TiO_2-SiO_2 NCs with varying composition. The size of the TiO_2 NPs was between 4 nm for low fraction of TiO_2 in the NC and increased up to 10 nm for higher compositions. Using ellipsometry and Lorentz-Lorentz effective medium

approximation this author showed that as the fraction of TiO_2 increases the refractive index and in addition, the porosity of the film increases. [41,42] In a similar way, Lopes de Jesus et al. [43] investigated both the porosity and the effective refractive index of the films using sol-gel derived TiO_2-SiO_2 NCs. Using Bruggeman effective medium approximation, it was possible to show the modulation of the refractive index (from 2.08 to 1.44 at $\lambda = 633$ nm), by varying the composition of the NC or its thickness (layered deposition with dip casting).

Based on these findings, the ability to choose the nature of the nanoparticles and more importantly their filling factor and size in the matrix is of great interest, as both the electrical and optical characteristics of the nanocomposite can be tuned in a controlled manner.

3 Processes for the preparation of Nanocomposite thin films and Nanomaterials

One of the most significant challenge in the development of such nanocomposites is the control of the growth mechanisms, the final morphology and the spatial distribution of the nanoparticles using reproducible, versatile and low-cost processes. Since nanocomposites and nanomaterials are an emerging scientific and industrial field, several approaches enable their production. A good discrimination could be the bottom-up and top-down ones. [44]

In this Section we have decided to separate the processes for the creation of nanomaterials in three general categories: approaches involving the precursors to be processed in (i) the liquid-phase, (ii) the gas-phase and (iii) both the liquid- and gas- phases. We denote the latter process the hybrid approach since it is coupling the two previous ones.

3.1 Liquid-Phase Processes

The term “liquid-phase” is used, to describe the condition when wet chemistry is carried out for the fabrication of the nanomaterials. One of the most widely used process for the creation of nanomaterials is sol-gel. The sol-gel process is a chemical synthesis that starts from an ionic or a molecular compound and forms a three-dimensional network through oxygen or hydroxyl bond formation between the ions and the release of water or other small molecules. Some advantages of this technique are the low temperature during the process, the widely used precursors and the reproducibility. On the other hand, when drying (to

create nanocomposite films), nanoparticles may be released arising several toxicity issues. [20,36] In case films are targeted, drying needs to be perfectly controlled in order to avoid cracks.

In more detail, sol-gel process is a chemical method which is based on hydrolysis and condensation reactions. [44–47] With the correct amount of reactants, nanosized particles nucleate. There are three basic steps in the sol-gel process: a) the partial hydrolysis of the reactant that can be metal alkoxides (a widely used precursor given as an example here) to form reactive monomers, b) the condensation of these monomers to form colloid-like polymers (sol formation). At this step, the hydrolysis and condensation reactions lead to the formation of solid particles that are suspended in the liquid, a so-called sol. Depending on the surface charge of the objects, the sol is stable if the zeta potential lies above 30 mV in absolute values. As the third step, the particles contain on their surface groups still active in condensation steps and therefore, they crosslink to a gel. The latter is defined as a solid network that contains liquid in its pores [48]. The last step involves drying the gel. Consolidation can be obtained by annealing at high temperature if densification is needed to lead either to films, fibres or powders.

Figure 3 shows schematically all the steps needed to acquire a nanomaterial through sol-gel. As this technique has been investigated since the middle of the 19^{th} century [49], there have been, as expected, numerous reports. Focusing on the materials of interest, meaning TiO_2 and SiO_2, such reports target mainly on their photocatalytic [50–54], antireflective [24,53,55], hydrophobic [56,57] and dielectric [38] properties. To attain the final nanocomposite, three main experimental processes were followed. The preparation of two different sols and the mixture of them [24,51,52,58], the preparation of TiO_2 sol and the mixture with an alkoxide such as tetraethoxysilane (TEOS- SiO_2 precursor) [55–57] or the mixture of TiO_2 NPs inside the TEOS precursor [54].The deposition of the produced nanocomposite sol-gel is taking place through spin coating, dip casting or drop casting.

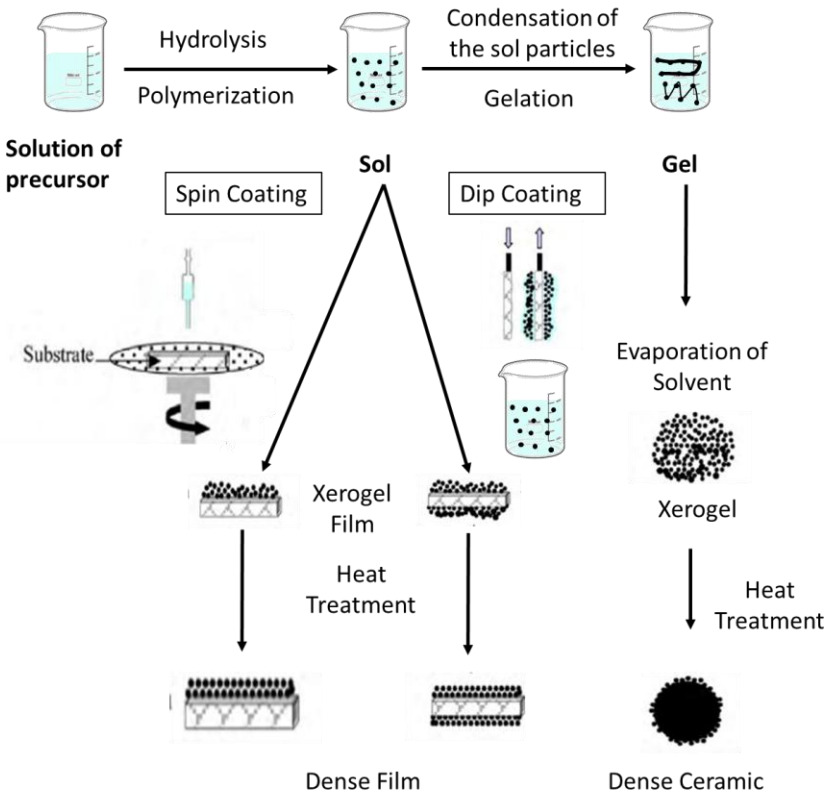

Figure 3: Different sol-gel process steps to control the final morphology of the product. Adapted from [59,60].

3.2 Gas-Phase Processes

The term "gas-phase" is used, to describe the state of the precursors in these processes being in a vapour or initially solid state inside the reactor/system.

Fanelli and Fracassi divided these processes in three categories. First, systems that use the same chemical source and strategy for the creation of NCs. This could be for example one Plasma Enhanced Chemical Vapour Deposition (PECVD) system using a mixture of precursors. This, may lead in the production of mixed oxide one-phase films, rather than a nanocomposite. In case these processes take place separately, then for instance TiO_2 NPs could be deposited through atmospheric pressure plasma based systems[61–64] and SiO_2/SiOX matrices through low pressure plasma based ones[65–69]. Second, the deposition using two independent chemical sources with one strategy such as co-sputtering [70], or co-evaporation [71]. Finally, the third category, where separated strategies and different sources are being followed. Over the last years, this category was proven more versatile in regard to the nature of the NPs and the matrix thus focusing more the attention of the scientific community. Hence, for the elaboration of

nanocomposite films through this category of processes, a combination of deposition systems is used for the simultaneous or step-by-step creation of the NPs and the matrix. For instance, in the past, several works involved the combination of Physical Vapor Deposition (PVD) and the Plasma Enhanced Chemical Vapor Deposition (PECVD) for the simultaneous deposition of the NPs and the matrix accordingly. [72–75] For the deposition of the NPs, sputtering-deposition techniques have been utilized such as DC glow discharges, capacitively coupled RF discharges, DC/RF magnetron plasma sources. Typical examples of successfully developed films consisting of metallic (e.g., Ag, Au, Pt, Ti) or metal oxide (e.g., SiO_2, TiO_2, ZnO) NPs embedded in a large variety of polymeric matrices have been reported through these approaches. [39]

More recently, Gas Aggregation nanocluster Sources (GAS) have been used for the preparation of metal [76–82] or metal oxide nanoparticles such as TiO_2 ones [83–86], mainly based on vacuum metal evaporation or magnetron sputtering. This takes place in an aggregation chamber enclosed by an orifice through which the expanding gas (usually an inert gas such as Ar or N_2) carries the clusters into the low pressure deposition chamber (typically Ultra High Vacuum one). [87] This process can then be used for the synthesis of the matrix using for instance plasma processes or using another magnetron configuration to create core-shell nanoparticles.

An example of gas-phase approaches is given in Figure 4. In this figure three different experimental strategies are followed for the creation of Ag/plasma polymer nanocomposites. In Figure 4a, the simultaneous sputtering and plasma polymerization of the NCs, in Figure 4b the deposition of the NCs from two independent magnetrons (having the possibility to adjust the experimental conditions/characteristics both of the NPs and the matrix), and in Figure 4c a combination of a gas aggregation source and plasma polymerization.

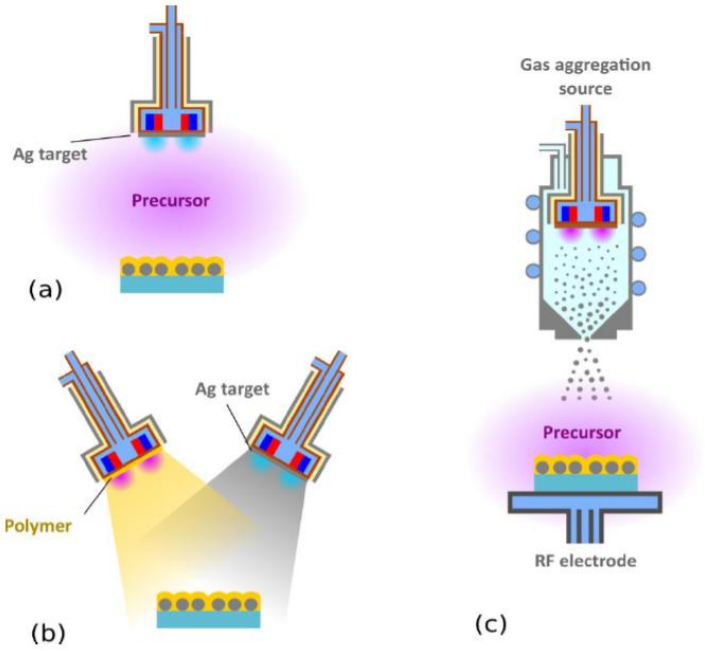

Figure 4: Different approaches for the production of Ag/plasma polymer nanocomposites: (a) Simultaneous sputtering and plasma polymerization, (b) deposition from two independent magnetrons, and (c) a combination of a gas aggregation source and plasma polymerization. Reproduced from [88], open source MDPI Publishing.

Some appealing characteristics of these gas-phase approaches are the high purity of the synthetized NPs and the environmentally friendly character (since no solvent or liquid precursors are needed). Contrary to that, the control of the NPs' characteristics is dependent on the system parameters with a small freedom for parametrization.

3.3 Hybrid Approaches coupling liquid and gas phase processes

Several liquid- and gas-phase processes aim in the elaboration of nanomaterials or nanocomposite thin films. The drawback of liquid-phase processes such as sol-gel is related to its multiple steps until acquiring a nanocomposite thin film as well as the toxicity that the NPs can have during the drying of the film. [44] Moreover, through gas phase processes, it has been shown that a combination of vacuum techniques is being used. This allows the simultaneous creation of the nanoparticles and optionally the matrix without the actual manipulation of the nanoparticles by the user. Unfortunately, the size, form and other parameters of the produced nanoparticles are difficult to control.

Hence, recently, an increasing trend has appeared from the scientific community aiming to the production of nanomaterials or nanocomposite thin films, by combining liquid and gas-phase processes. This is attempted by creating an aerosol of the NPs colloidal solution or directly injecting the colloidal solution inside a gas-phase system. The flexibility offered by aerosol-assisted deposition processes, in respect to those in which NPs are generated *in situ*, mainly resides in the possibility of using many preformed NPs in combinations with any compatible conventional precursor. [39]

The challenging part in approaches like these mainly lies in the droplet or aerosol production. Hence, a specific system will be needed to allow this droplet production in atmospheric or low-pressure gas-phase systems. Thanks to the spray drying [89,90] techniques, spray pyrolysis [91–93] or analytical techniques, such as inductively coupled plasma optical emission spectrometry and mass spectrometry (ICP-OES, ICP-MS) [94–98], the adaptation of these systems could be possible. Several droplet generation techniques exist involving different driving force to assist the droplet formation such as vaporization, pressure, centrifugation, electrostatic forces, and ultrasonic atomization. [89]

In this section, these hybrid configurations will be introduced, being categorized by the working pressure of the gas process system (atmospheric or low pressure). At the end of this Section, an accumulative table with the hybrid approaches used and the film characteristics will be given in order to make a qualitative assessment of the produced films.

3.3.1 Atmospheric Pressure based systems

Several attempts have been published over the past ten years aiming in the deposition of either nanoparticles only or nanocomposite thin films using hybrid approaches. In this part, some of the atmospheric pressure configurations will be analysed along with their injection system. Three main categories were reported in the literature:the Suspension Plasma Spray, the systems using non-equilibrium atmospheric pressure Plasma Jets and the ones using Dielectric Barrier Discharges (DBD).

Regarding the first category, the Suspension Plasma Spray [99–102], utilizes the high temperature and high velocity plasma jet to melt and spray nanometer-sized nanoparticles. Each drop of the liquid stream is fragmented into droplets (< a few μm), which, after vaporization of the liquid phase, result in nano- or sub-micrometre-sized melted or partially melted particles, forming nanostructured coatings. [101] This process resembles the one of spray pyrolysis with the difference that the heat comes from the plasma

(temperature up to 10000 K) and not from a furnace. The resulted films have a melted like appearance with polydispersed in size deposited particles.

Moreover, the approaches using non-equilibrium Plasma Jet configuration usually involve a system where the working gas along with the matrix precursor and the nebulized liquid are fed to the Plasma Jet. [103–105] For instance, as described by Liguori et al. [105] and given schematically in Figure 5, at the same time the solution containing NPs is injected into the plasma source through the primary channel. Simultaneously, a second flow of Ar is introduced in a nebulizer system containing the dispersion of Ag NPs in ethanol (EtOH). The so-formed aerosol is injected into the plasma source through the secondary gas channel. The resulted films were polymerized polyacrylic acid (pPAA) and silver nanoparticles (around 100 nm in size) having antimicrobial applications, a SEM image of which can be seen in Table 1 (Ref. 90).

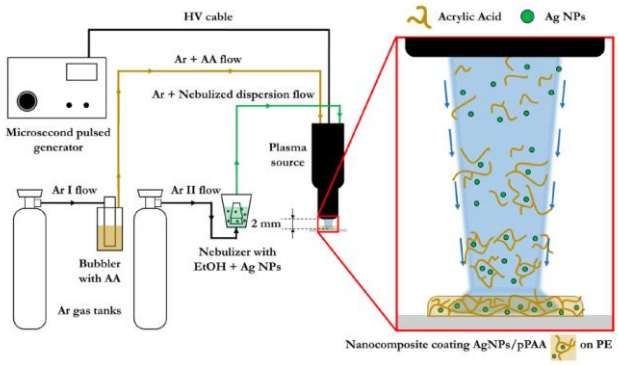

Figure 5: Experimental setup of the plasma co-deposition process. Reproduced with permission from [105], copyright 2015 John Wiley and Sons Publishing.

Since 2006 many reports involve the Dielectric Barrier Discharge (DBD) systems, for the injection of the colloidal solution and the deposition of nanomaterial thin films. [39,106–114] For the efficient preparation and injection of the liquid solution containing NPs, two main systems were used, which are the nebulizer and the atomizer. In the case of the nebulizer, the flow rate of the colloidal solution is fed to the nebulizer through its regulation by a syringe pump. There the carrier gas for the production of the aerosol is introduced and based on the Venturi effect, an aerosol is generated at the outlet of the nebulizer. [115] In the case of the atomizer, compressed air expands through an orifice to form a high-velocity jet. At the same time, the liquid is drawn into the atomizing section through a vertical passage and is then atomized by the air jet. [116] Recently, using a DBD system with a nebulizer, Profili at al. [110–113] reported several

experiments for the deposition of nanocomposite thin films using the DBD reactor given in Figure 6. This group attempted the deposition of TiO_2 NPs only or nanocomposite thin films through various approaches such as dissolving the NPs inside the Hexamethyldisiloxane (HMDSO) liquid and injecting it in the system (see Table 1, Ref 96 for the SEM images) or in a two-step approach injecting first the colloidal solution of NPs (see Table 1, Ref 95 for the SEM images) and second the SiO_2 matrix (introducing the vapour in the plasma).

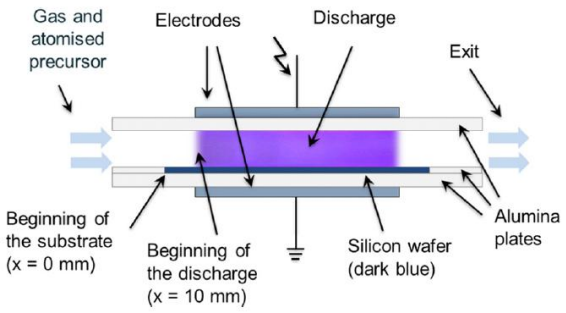

Figure 6: Schematic of the dielectric barrier discharge reactor used for the growth of nanocomposite thin films in the works [110–113]. Reproduced with permission from [111], copyright 2016 AIP Publishing.

3.3.2 Low-pressure-based systems

A small number of scientific reports have been published involving low-pressure physical systems. This could be due to the fact that handling of aerosols or liquids at low pressure is challenging. These challenging conditions can be for instance the reactor contamination especially when working at room temperature, the degradation of the turbopump lifetime and plasma perturbation (if there is use of plasma) due to pressure variation caused by the solvent vaporization. [39,117] Two main categories will be given here, the thermally activated vacuum techniques such as the Chemical Vapor Deposition (CVD) and the ones based on PECVD. Due to the scope of this work, the main focus will be given at the low-pressure plasma systems used, and their configuration to produce nanomaterials through this hybrid approach.

Some works involve the combination of the CVD systems with a direct liquid injector to produce nanomaterials. [118–120] An example of the configuration based on the direct liquid injection of the solvent containing nanoparticles is given in Figure 11a.

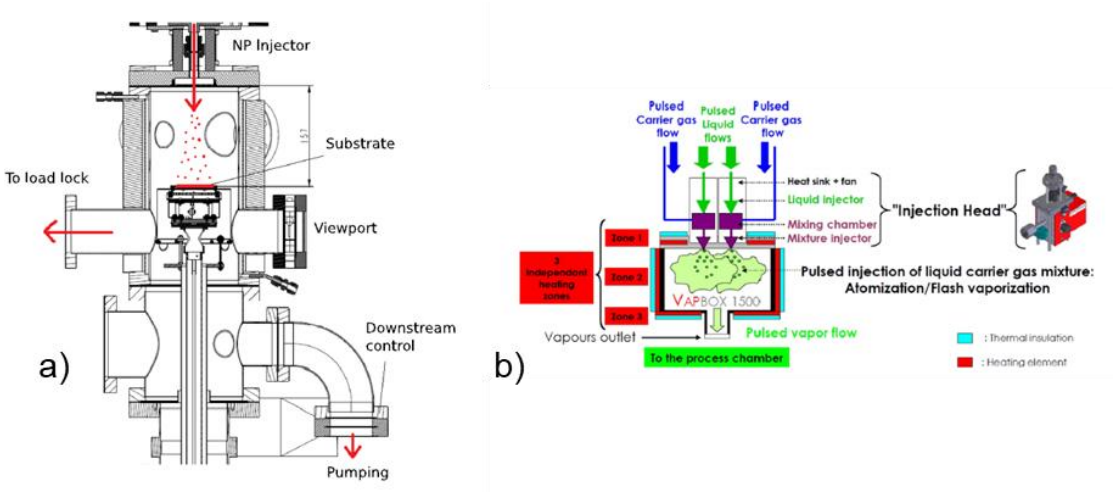

Figure 7: a) Schematic of the process chamber. b) Schematic of the Kemstream Vapbox 1500 injection head. Reproduced with permission from [120], copyright 2016 AIP Publishing.

As observed in this scheme (Fig 7a), the injector has been positioned at the top of the reactor facing the rotating substrate holder which is heated at 150 °C. This results in the deposition of gold nanoparticles whose size was found to depend on the flow rate of the injected solution (containing NPs). AFM scan of the deposited gold nanoparticles is given in Table 1, Ref 105. The gas used for this approach was N_2, in order to avoid any reactions with the gold NPs. In Figure 7b a detailed diagram of the injection system is given, being comprised of an atomizer and a heated chamber. This allows the production of the aerosol with the help of a carrier gas.

Additional works have been found using a similar direct liquid injection (DLI) system for CVD [121–123] and Atomic Layer Deposition (ALD) [124,125] systems but without though the presence of nanoparticles in the injected liquid. They only capitalize the DLI process to atomize the injected liquid, vaporize it and generate the reactive vapour.

The first report using a low pressure plasma system, aiming at the simultaneous injection of the NPs in a solution and the injection of the matrix precursor using the PECVD technique has been proposed by Ross et Gleason [126] in 2006. These authors report that the atomization of the solution is accomplished by a 40 kHz ultrasonic atomizer (Sonics and Materials, model VC134-AT with custom probe) located at the top of the reactor. The ultrasonic atomizers are based on the vibration of a quartz at high frequencies, typically 1 to 4 MHz. Vibrations created cause the surface liquid film to burst into very fine droplets. However, these devices are used in the case of a large flow of suspension. Through a distribution ring, the

matrix precursor (HMDSO) was introduced inside the reactor. The produced plasma was created using O_2 as a working gas and an RF power supply as shown in Figure 8.

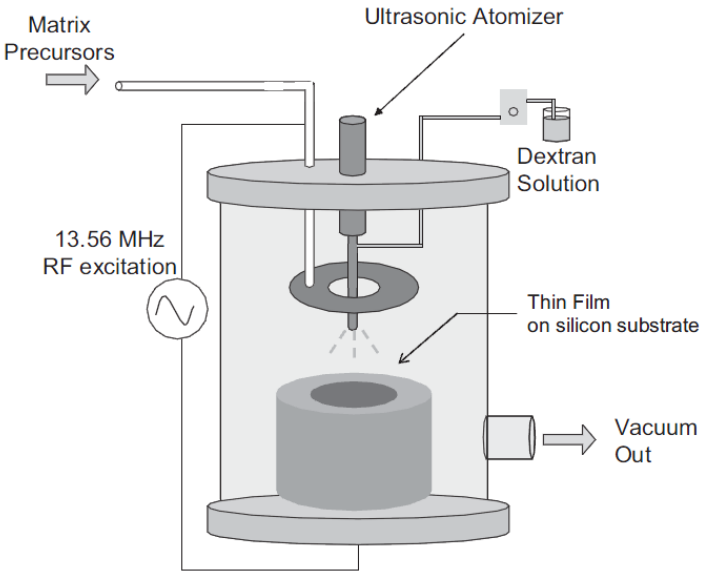

Figure 8: Reactor configuration for simultaneous plasma-enhanced deposition of matrix material and ultrasonic atomization deposition of particles. Reproduced with permission from [126], copyright 2006 John Wiley and Sons Publishing.

The plasma was pulsed at an on-off rate of 10–40 ms, with a peak power of 300 W. For the deposition, the pressure was maintained between 100-500 mTorr. The resulting films were polystyrene nanospheres with 96 nm diameter embedded inside the carbon-doped silicon dioxide matrix (see Table 1, Ref. 111). An interesting observation from this work was the appearance of droplets formed at the surface of the film. Hence, the first attempts investigating how the volatility of the solvents can improve this phenomenon were established using water, ethylene glycol and labelled dextran (for fluorescent microscopy).

Three years later, in 2009, Ogawa et al. [127] reported a complete experimental study of directly introducing the liquid inside the low pressure Ar Capacitively Coupled Plasma (CCP) powered by an RF power supply (Figure 9). This was established using a Denso fuel injector (23209-0D040) in a pulsed mode and a produced droplet diameter estimated at 50 µm. The deposited Fe nanoparticles (brown rings) using this approach can be seen in Table 1, Ref 114.

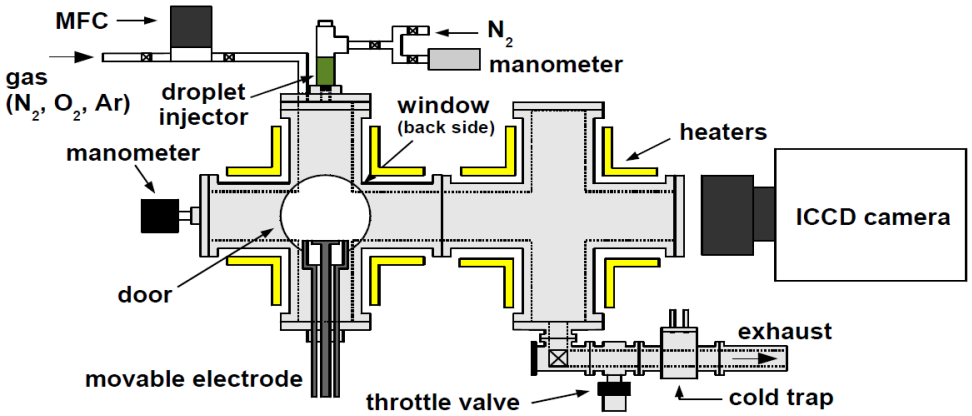

Figure 9: A schematic diagram of the experimental apparatus used in [127–129]. Reproduced from [129], Open Access IOP Publishing.

Furthermore, as discussed in a relative recent review of Bruggeman et al. [117] on plasma-liquid interactions, both the impact of the plasma to the droplets and vice versa has been poorly understood and studied. Ogawa's study was the first attempt to refer to the term "misty plasmas", being plasmas that contain liquid droplets. This term was first proposed by Coppins [130,131] in 2004. Coppins stated also that these misty plasmas would not differ significantly from the dusty plasmas (plasma containing millimeter to nanometer particles) but that the liquid state of the droplets could allow droplet deformation and make surface tension forces more important. On this basis, Ogawa attempted the creation of a model (Figure 14) describing the energy fluxes entering and exiting the droplet under the specific plasma conditions. Using this model and the energy balance equation he was able to determine the parameters affecting the droplet evaporation in this low-pressure medium. Finally, in a following work [128] he investigated the transient effects caused by the liquid injection on the same low pressure plasma.

Recently, Clergereaux's group [132,133] reported a new safer-by-design method for NC thin film plasma deposition. This method allowed them to synthesize NPs from organometallic precursor in the reactor-injector prior to their injection in the RF low-pressure (750 mTorr) plasma reactor. The resulted nanocomposites consisted of small (6 ± 3 nm) and isolated (i.e., non-aggregated) ZnO NPs homogeneously dispersed in an amorphous hydrogenated carbon matrix (SEM image on Table 1, Ref 117). As seen in the top of Figure 10, they were able to control the chemical synthesis of the NPs inside the reactor-injector and

the characteristics of the deposition, was controlled by the low-pressure plasma reactor. During this work, studies to investigate the pulsed injection impact on the plasma were carried out.

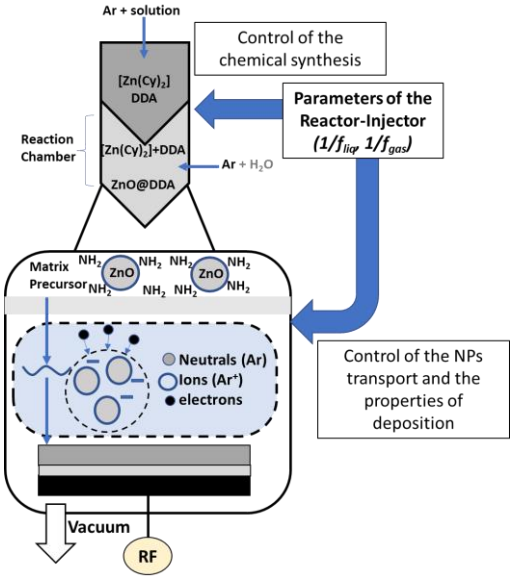

Figure 10: Reactor-injector and RF low-pressure plasma system used by Carnide et al. Adapted with permission from [132].

As for the most recent reports, our group [134] attempted for the first time the pulsed injection of the colloidal solution (lab-made) [135] [136] in much lower pressure plasma system such as 3 mTorr. The objective of this study was to elaborate TiO_2-SiO NC thin films though a versatile and agile hybrid process. The interest of very low pressure in terms of plasma species lies in the possibility to finely control the growth of the silica matrix in which exhibits a high optical quality. To achieve the NCs synthesis, in a low pressure PECVD system, a Kemstream liquid doser was mounted as shown in the experimental setup provided in Figure 11a,b. The injection sequence was optimised to allow the solvent to be fully oxidised and the pressure to be maintained in a low range. Each sequence lasted one minute during which N pulses of 1 ms injection separated by 2 s OFF time were performed, with N =0, 2, 10, 30. This sequence was repeated for a controlled duration. The cross section of the film (see Table 1, Ref. 119) revealed a fairly homogeneous distribution of the NPs inside the matrix, at the local scale. Among others, the most prominent and promising result from this work, was the fact that adjusting the parameters of the injection sequence (from N = 2 to N = 30), NC films with lower and higher TiO_2 NPs content (7 to 53 %) and thus different optical properties (refractive index 1.50 to 1.74) could be achieved.

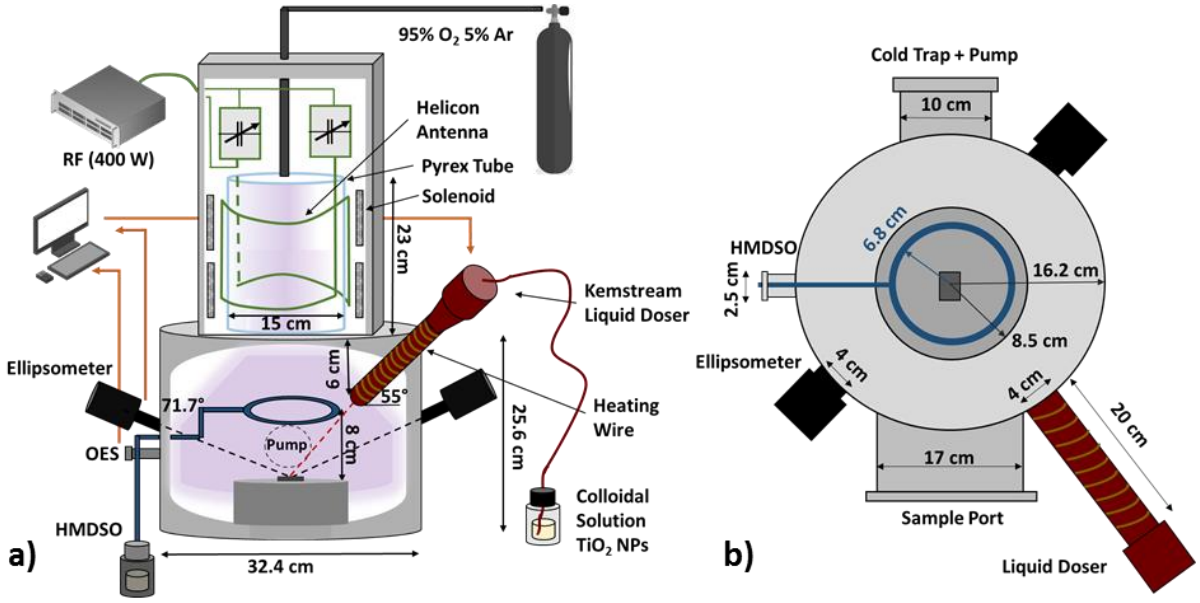

Figure 11: Schematic of the hybrid experimental setup including the low pressure ICP O_2 reactor, the liquid doser apparatus (with red) and the HMDSO vapor distribution system (with bleu) at a) side view and b) top view. The *in situ* characterization techniques are also indicated on this schematic. Reproduced from [134], copyright 2021 IOP Publishing.

3.3.3 Characteristics of the produced nanomaterials through the hybrid approaches

Due to the originality of this hybrid approach coupling the gas and liquid phase processes, Table 1 was produced, indicating a majority of the works since 2006. In this table, details regarding the process parameters, the system used, the precursors and working pressure are given. Moreover, the characteristics of the produced films and the evolution of the NPs size upon deposition are discussed.

Table 1: Comparative table of the hybrid systems used and the characteristics of the produced nanomaterials. Images reproduced with permission from each Publishing Organization.

System Configuration	Precursors	Pressure	NPs evolution during deposition	Produced nanomaterial	View of the Nanomaterials	Ref.
Ar Plasma Jet + nebulizer	Admixtures with alcohols for solution stability TiO_2 NPs/ tetramethoxysilane, TMOS/methanol TiO_2 NPs /TMOS/pentanol TiO_2 NPs/ TMOS/octanol NPs Origin: Commercial	Atm.	Initially: 30–80 nm After Deposition: 50-700 nm	Hybrid Organic–Inorganic Composite	TiO_2 NPs/TMOS/methanol *Cf. the original work*	[103]
Ar Plasma Jet +nebulizer (Ar carrier gas)	Acrylic Acid + Ag NPs in ethanol, EtOH (Co-deposition) NPs Origin: Commercial	Atm.	Initially: (mean diameter<100 nm After Deposition: characteristic dimension around 100 nm	0.9 at.% Ag NPs in polymerized polyacrylic acid (pPAA)	AgNPs/pPAA 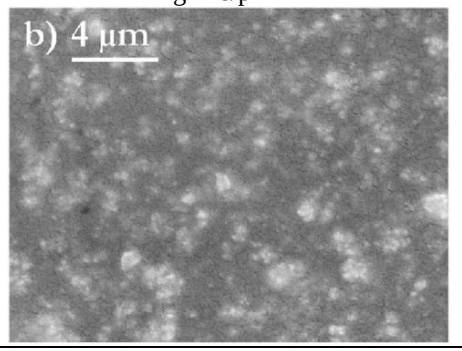	[105]

Ar DBD + nebulizer(Ar carrier gas)	CuO nanoparticles are suspended in acetone or methyl methacrylate (MMA) NPs Origin: -	Atm.	Initially: 30 nm After Deposition: Agglomerated and single needle like particles 200-500 nm	CuO NPs with a carbon coating	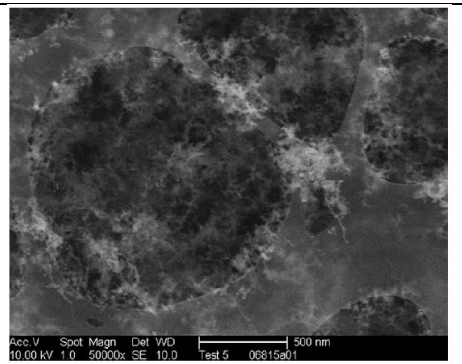	[106]
DBD +atomizer (N_2/O_2 carrier gas)	$AlCeO_3$ in HMDSO solution and admixture with ethanol to improve NPs distribution NPs Origin: Commercial	Atm.	Initially: 25 – 200 nm After Deposition: -	1-4% AlCeO3 NPs (agglomerates) in ppHMDSO matrix (NC)	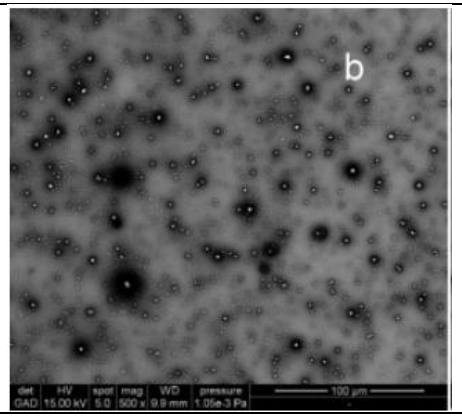	[107]
	$AlCeO_3$ in HMDSO solution NPs Origin: Commercial	Atm.	Initially: 25 – 200 nm After Deposition: 100 nm to several µm	1-4% AlCeO3 NPs (agglomerates) in ppHMDSO matrix (NC)	*Cf. the original work*	[108]
He DBD + pneumatic atomizer (He carrier gas)	ZnO NPs in n-octane solution NPs Origin: Commercial	Atm.	Initially: ~36 nm After Deposition: ~640 nm	ZnO NPs (agglomerates) polyethylene-like polymer matrix (NC) -The NPs concentration varied in the solution, 0.5 to 5 wt %. Led 0.5% -4.5 at% and 19 ± 3 wt % to 78 ± 4 wt % loading.	Oleate-capped ZnO NPs in n-octane at a concentration of 0.5, 3, and 5 wt % (deposition time = 10 min)	[109]

					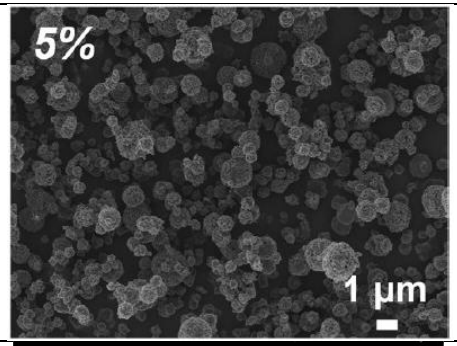	
DBD + nebulizer (N2 + N2O carrier gas)	HMDSO in vapor + TiO2 NPs colloidal suspension	Atm.	Initially: ~30 nm with some agglomerates 100 nm After Deposition: 100 nm range	2 step deposition of TiO_2 NPs and silica like matrix (NC)	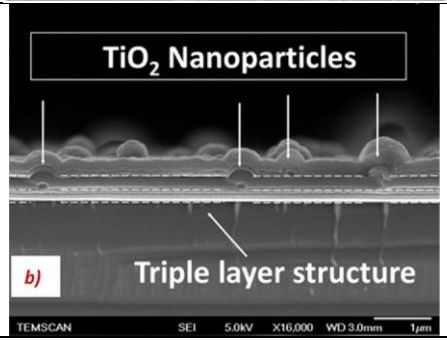	[110]
	TiO_2 NPs colloidal suspension in HMDSO NPs Origin: Lab-made	Atm.	Initially:20–120 nm After Deposition: 30–500 nm	TiO_2 NPs 3% in weight (agglomerates) in silica-like matrix (NC)	(NPs) TiO_2 NPs in H_2O 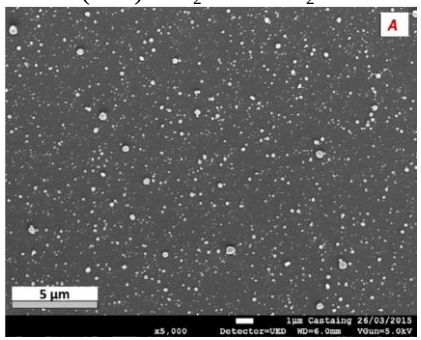	[111]

					(NC) TiO_2 NPs in HMDSO+EtOH 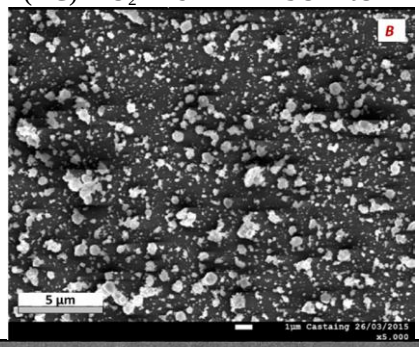	
	ZnO NPs in pentane+HMDSO solution NPs Origin: Commercial	Atm.	Initially: 7.7 nm, FWHM of 6 nm After Deposition: agglomeration Due to agglomeration in the suspension when HMDSO is added	ZnO NPs (agglomerates) in silica-like matrix (NC)		[112]
	TiO_2 NPs in water	Atm.	TiO_2 NPs Interaction of atomized colloid with the DBD AC electric field. Effect on their size distribution		No image reported	[113]
DBD + nebulizer (Ar carrier gas)	TiO_2 NPs coated by TMOS added to 50 ml of isopropanol (IPA) NPs Origin: Commercial	Atm.	Initially: 20 nm After Deposition: clusters with ~25 nm	TiO_2 NPs in a polymer matrix (NC) NPs only: Increasing the power supply frequency from 1 to 50 kHz, a decrease on the NPs coverage is observed. At % from 23 to 0.5 for the Ti content (XPS)	TiO_2 NPs @1 kHz AC 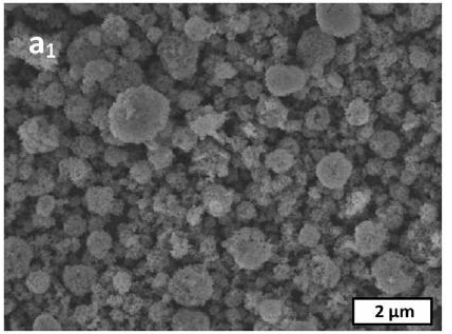	[114]

MOCVD + Kemstream (N_2 carrier gas)	TTiP vapor + □-Al_2O_3 in isopropyl alcohol solution NPs Origin: Commercial	7.5 Torr	Initially: 40 nm After Deposition: 1245 ± 75 nm (aggregates)	a-Al_2O_3 particles in TiO_2 matrix (NC)	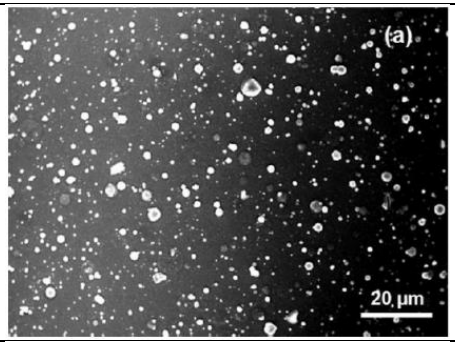	[119]
CVD + Vapsoft 1500 Kemstream (N_2 carrier gas)	Gold NPs in solution [137] NPs Origin: Lab-made	-	Initially: 2 ± 0.6 nm. After Deposition: 5.2 ± 1 nm.	Gold NPs Solvent mass rate affects the NPs size (agglomerates)	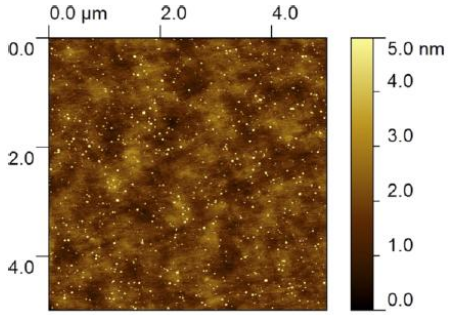	[120]
Low Pressure O_2 Plasma + 40 kHz ultrasonic atomizer	Tetraethoxysilane, TEOS in vapor (PECVD) + dextran/ aqueous dextran/ ethylene glycol polystyrene NPs/aqueous suspensions NPs Origin: Commercial	100-500 mTorr	Initially: 96 ± 9 nm. A variation on the size upon deposition was not observed	carbon-doped silicon dioxide (OSG) matrix, polystyrene NPs 96 nm (NC)	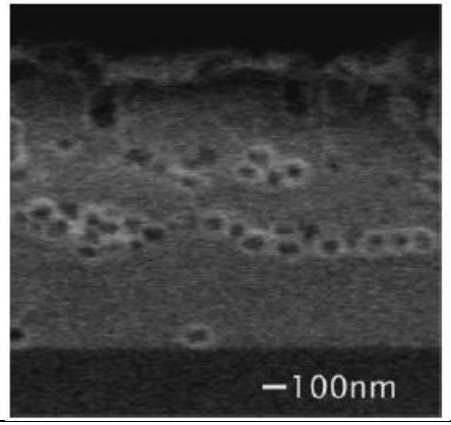	[126]

Low Pressure Ar Plasma + Fuel Injector	Fe NPs in hexane solution NPs Origin: -	400 mTorr	Initially: 2 nm After deposition: agglomerations range from 2 to 20 µm	Fe fraction per unit volume ~ 3.9% in hydrocarbon matrix	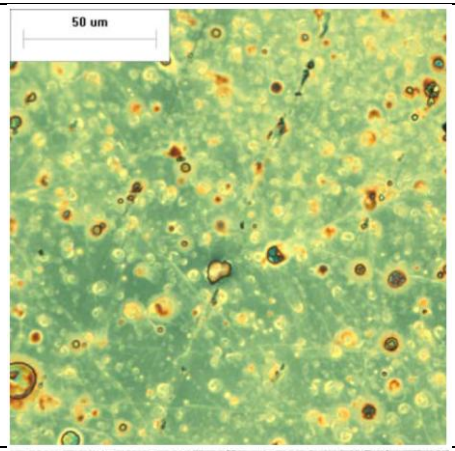	[129]
Low Pressure Ar plasma + reactor-injector	$Zn(C_6H_{11})_2$ + H_2O in Pentane, Cyclohexane, Toluene or Heptane NPs Origin: Lab-made	750 mTorr	Initially: liquid precursor After deposition: 6 ± 3 nm	ZnO NPs in an amorphous hydrogenated carbon matrix. Small mean diameter size and homogeneous distribution.	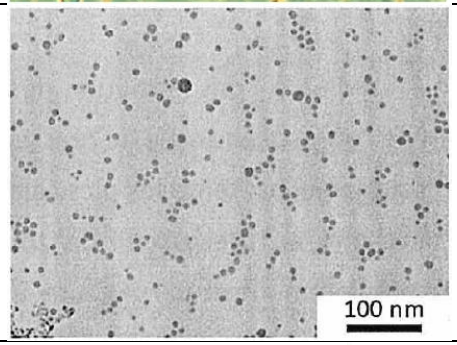	[132,133]
Low Pressure + O_2 Plasma + HMDSO vapor precursor +Kemstream Liquid Doser	TiO_2 NPs in colloidal solution solution [138–140] NPs Origin: Lab-made	3 mTorr	Initially: 2.7 nm After deposition: 2.7 ± 0.4 nm	TiO_2 NPs distributed in SiO_2 matrix	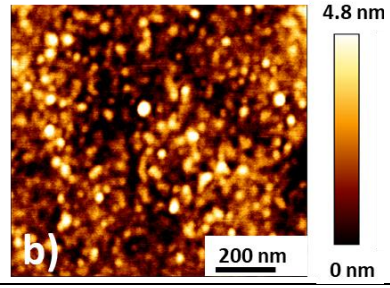	[134]

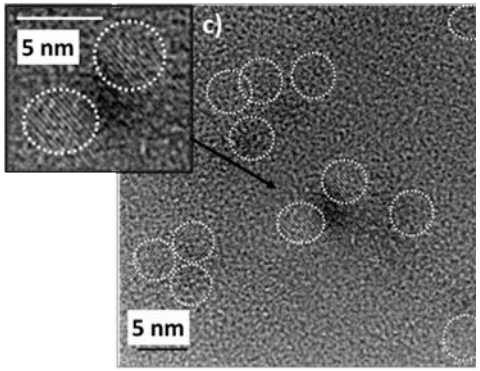
5 nm
c)
5 nm

A first observation from this table is that the majority of the provided works were conducted at atmospheric pressure. This could be linked to the relative easier set up as there is no turbomolecular pump and the injection of the aerosol is facilitated by the geometry of the system and the gas flow configuration. The preponderant use of DBD configurations over plasma jets could be linked to the lower temperature the first exhibits, and the possibility to deposit over higher surface area. Additionally, DBD have the unique and main advantage of being cold plasmas (namely out of local thermodynamic equilibrium) created at atmospheric pressure. In other words, a lot of similarities with low pressure plasmas but without huge pumping device. It remains nevertheless one difference between low pressure plasmas and DBD, due to high pressure which is the low ion energy and very small mean free paths which limit the possibility of depositing dense films and can limit the homogeneity (in terms of thickness and composition, independently of the NC dispersion) On the other hand, it is suited for deposition on planar substrates but not on other geometries. An issue occurring frequently in these works is the agglomeration of the initial NPs upon deposition. Some more recent works, such as from Profili et al. [113] investigated the impact of the ac voltage parameters of the DBD power supply on the deposited size distribution of the NPs. In addition to this, regarding the low pressure system Vervaele et al. [120] showed that for a low pressure CVD system, the mass flow rate of the introduced solvent significantly affects the size of the deposited NPs. Furthermore, three general categories of experimental strategies were identified for the production of nanomaterials. First, the NPs colloidal solution was injected only in the plasma system for the deposition of NPs. In this scenario, when the solvent is organic, a carbon-like matrix could be observed surrounding the NPs. Second, for the creation of NC thin films, the NPs were dissolved in the liquid precursor of the matrix. Third, the deposition of the matrix precursor and the NPs took place from two separate sources. Three works were identified with the latter experimental strategy. The first by Profili et al. [110] where two steps were followed namely the deposition of the TiO_2 NPs (from the aerosol) and after the injection of the HMDSO vapor precursor in the DBD reactor. The created film was a layered nanocomposite. The second work was from Ross et Gleason [126] where the colloidal solution with the NPs was injected simultaneously with the HMDSO vapor precursor in the low pressure (100-500 mTorr) plasma reactor (RF CCP). The third work was from our group [134] where the TiO_2 NP colloidal solution was introduced simultaneously with the HMDSO vapor precursor of the matrix in the low pressure 3 mTorr O_2 plasma reactor (RF ICP).

From the characteristics regarding the produced nanomaterials in Table 1, it appears that the majority of the works have an organic matrix. This could be linked with the transient effects happening during the liquid

vaporization (pressure variation, discharge perturbation etc) or the released organic species that can affect the inorganic quality of the deposited matrix (in case it is preferred for the application of the produced films). Finally, the concentration of the distributed NPs has propelled the curiosity of the researchers. For the majority of the works the NPs content remains in low levels (less than 5%). Brunet et al. [114] attempted to control the coverage percentage through the power supply frequency of the DBD (adjusting the process) whereas Fanelli et al. [109] chose to increase the NPs concentration in the solution (by adjusting the precursor). Finally, we [134] showed that it was possible through a specific approach and particularly by optimising the sequence of injection to tune the TiO_2 NPs content up to 58% while achieving tuneable optical properties of the film.

3. Conclusion

The aim of this review paper was to gather novel approaches for the deposition of NC thin films, based on the coupling of liquid and gas phase deposition processes. While oxide-based NC thin films (such as TiO_2-SiO_2 NCs) have several attractive applications, most of the works discussed in this review also include an organic matrix. This is linked to the novel character of these approaches and the complex phenomena induced when liquid and more specifically an organic solvent is introduced in gas phase deposition systems. From this detailed comparative overview, the challenges and difficulties to develop NC films, retaining the initial mono dispersity in size of the NPs, with controlled composition and homogeneous NPs dispersion in the matrix through plasma-based hybrid processes is clearly highlighted. Additionally, it is evidenced that approaches like these lack in computational and theoretical studies, which can be proven crucial for the optimization of the reported experimental setups. Finally, the paramount objective of these approaches is the ability to create an agile process, through which, it can be possible to tune and adjust the properties of the NC film, with a high degree of freedom.

4. Acknowledgments

The authors would like to thank Professor Luc Stafford and Dr. Jacopo Profili for their discussions regarding atmospheric pressure DBD hybrid systems.

3. Ethics declarations

Conflicts of interest

On behalf of all authors, the corresponding author states that there is no conflict of interest.

References

1. *Dielectric Polymer Nanocomposites*; Nelson, J.K., Ed.; Springer: New York, 2010; ISBN 978-1-4419-1590-0.
2. Pokropivny, V.V.; Skorokhod, V.V. Classification of Nanostructures by Dimensionality and Concept of Surface Forms Engineering in Nanomaterial Science. *Mater. Sci. Eng. C* **2007**, *27*, 990–993, doi:10.1016/j.msec.2006.09.023.
3. Jeevanandam, J.; Barhoum, A.; Chan, Y.S.; Dufresne, A.; Danquah, M.K. Review on Nanoparticles and Nanostructured Materials: History, Sources, Toxicity and Regulations. *Beilstein J. Nanotechnol.* **2018**, *9*, 1050–1074, doi:10.3762/bjnano.9.98.
4. Sanchez, C.; Julián, B.; Belleville, P.; Popall, M. Applications of Hybrid Organic–Inorganic Nanocomposites. *J. Mater. Chem.* **2005**, *15*, 3559, doi:10.1039/b509097k.
5. Zhang, X.-Y.; Li, H.-P.; Cui, X.-L.; Lin, Y. Graphene/TiO2 Nanocomposites: Synthesis, Characterization and Application in Hydrogen Evolution from Water Photocatalytic Splitting. *J. Mater. Chem.* **2010**, *20*, 2801, doi:10.1039/b917240h.
6. Rhim, J.-W.; Park, H.-M.; Ha, C.-S. Bio-Nanocomposites for Food Packaging Applications. *Prog. Bionanocomposites Green Plast. Biomed. Appl.* **2013**, *38*, 1629–1652, doi:10.1016/j.progpolymsci.2013.05.008.
7. Dong, H.; Wu, Z.; Lu, F.; Gao, Y.; El-Shafei, A.; Jiao, B.; Ning, S.; Hou, X. Optics–Electrics Highways: Plasmonic Silver Nanowires@TiO 2 Core–Shell Nanocomposites for Enhanced Dye-Sensitized Solar Cells Performance. *Nano Energy* **2014**, *10*, 181–191, doi:10.1016/j.nanoen.2014.09.011.
8. Xu, J.; Wang, Y.; Hu, S. Nanocomposites of Graphene and Graphene Oxides: Synthesis, Molecular Functionalization and Application in Electrochemical Sensors and Biosensors. A Review. *Microchim. Acta* **2017**, *184*, 1–44, doi:10.1007/s00604-016-2007-0.
9. Müller, K.; Bugnicourt, E.; Latorre, M.; Jorda, M.; Echegoyen Sanz, Y.; Lagaron, J.; Miesbauer, O.; Bianchin, A.; Hankin, S.; Bölz, U.; et al. Review on the Processing and Properties of Polymer Nanocomposites and Nanocoatings and Their Applications in the Packaging, Automotive and Solar Energy Fields. *Nanomaterials* **2017**, *7*, 74, doi:10.3390/nano7040074.
10. Rao, Y.; Chen, S. Molecular Composites Comprising TiO_2 and Their Optical Properties. *Macromolecules* **2008**, *41*, 4838–4844, doi:10.1021/ma800371v.
11. Belka, R. Analysis of Optical Properties of Fullerene-Palladium Nanostructures Using Effective Medium Theory.; Romaniuk, R.S., Ed.; Wilga, Poland, October 25 2013; p. 89030B.
12. Garahan, A.; Pilon, L.; Yin, J.; Saxena, I. Effective Optical Properties of Absorbing Nanoporous and Nanocomposite Thin Films. *J. Appl. Phys.* **2007**, *101*, 014320, doi:10.1063/1.2402327.
13. Lozovski, V.; Strilchuk, G. Optical Properties of Nanocomposite Films with Inclusions of the Same Dimensions as the Film Thickness. In Proceedings of the 2015 IEEE 35th International Conference on Electronics and Nanotechnology (ELNANO); IEEE: Kyiv, Ukraine, April 2015; pp. 158–160.
14. Khan, I.; Saeed, K.; Khan, I. Nanoparticles: Properties, Applications and Toxicities. *Arab. J. Chem.* **2017**, *12*, 908–931, doi:10.1016/j.arabjc.2017.05.011.
15. Sarkar, D.K.; Brassard, D.; Khakani, M.A.E.; Ouellet, L. Dielectric Properties of Sol–Gel Derived High-k Titanium Silicate Thin Films. *Thin Solid Films* **2007**, *515*, 4788–4793, doi:10.1016/j.tsf.2006.11.155.
16. Brassard, D.; Sarkar, D.K.; El Khakani, M.A.; Ouellet, L. Compositional Effect on the Dielectric Properties of High-k Titanium Silicate Thin Films Deposited by Means of a Cosputtering Process. *J. Vac. Sci. Technol. Vac. Surf. Films* **2006**, *24*, 600–605, doi:10.1116/1.2180267.
17. Li, D.; Carette, M.; Granier, A.; Landesman, J.P.; Goullet, A. Effect of Ion Bombardment on the Structural and Optical Properties of TiO 2 Thin Films Deposited from Oxygen/Titanium

Tetraisopropoxide Inductively Coupled Plasma. *Thin Solid Films* **2015**, *589*, 783–791, doi:10.1016/j.tsf.2015.07.015.
18. Li, D.; Bulou, S.; Gautier, N.; Elisabeth, S.; Goullet, A.; Richard-Plouet, M.; Choquet, P.; Granier, A. Nanostructure and Photocatalytic Properties of TiO2 Films Deposited at Low Temperature by Pulsed PECVD. *Appl. Surf. Sci.* **2019**, *466*, 63–69, doi:10.1016/j.apsusc.2018.09.230.
19. Jolivet, J.-P.; Cassaignon, S.; Chanéac, C.; Chiche, D.; Durupthy, O.; Portehault, D. Design of Metal Oxide Nanoparticles: Control of Size, Shape, Crystalline Structure and Functionalization by Aqueous Chemistry. *Comptes Rendus Chim.* **2010**, *13*, 40–51, doi:10.1016/j.crci.2009.09.012.
20. Auffan, M.; Pedeutour, M.; Rose, J.; Masion, A.; Ziarelli, F.; Borschneck, D.; Chaneac, C.; Botta, C.; Chaurand, P.; Labille, J.; et al. Structural Degradation at the Surface of a TiO_2 -Based Nanomaterial Used in Cosmetics. *Environ. Sci. Technol.* **2010**, *44*, 2689–2694, doi:10.1021/es903757q.
21. Jamuna-Thevi, K.; Bakar, S.A.; Ibrahim, S.; Shahab, N.; Toff, M.R.M. Quantification of Silver Ion Release, in Vitro Cytotoxicity and Antibacterial Properties of Nanostuctured Ag Doped TiO2 Coatings on Stainless Steel Deposited by RF Magnetron Sputtering. *Vacuum* **2011**, *86*, 235–241, doi:10.1016/j.vacuum.2011.06.011.
22. Homola, T.; Shekargoftar, M.; Dzik, P.; Krumpolec, R.; Ďurašová, Z.; Veselý, M.; Černák, M. Low-Temperature (70 °C) Ambient Air Plasma-Fabrication of Inkjet-Printed Mesoporous TiO_2 Flexible Photoanodes. *Flex. Print. Electron.* **2017**, *2*, 035010, doi:10.1088/2058-8585/aa88e6.
23. O'Regan, B.; Grätzel, M. A Low-Cost, High-Efficiency Solar Cell Based on Dye-Sensitized Colloidal TiO2 Films. *Nature* **1991**, *353*, 737–740, doi:10.1038/353737a0.
24. Adak, D.; Ghosh, S.; Chakrabarty, P.; Mondal, A.; Saha, H.; Mukherjee, R.; Bhattacharyya, R. Self-Cleaning V-TiO 2 :SiO 2 Thin-Film Coatings with Enhanced Transmission for Solar Glass Cover and Related Applications. *Sol. Energy* **2017**, *155*, 410–418, doi:10.1016/j.solener.2017.06.014.
25. Adak, D.; Ghosh, S.; Chakraborty, P.; Srivatsa, K.M.K.; Mondal, A.; Saha, H.; Mukherjee, R.; Bhattacharyya, R. Non Lithographic Block Copolymer Directed Self-Assembled and Plasma Treated Self-Cleaning Transparent Coating for Photovoltaic Modules and Other Solar Energy Devices. *Sol. Energy Mater. Sol. Cells* **2018**, *188*, 127–139, doi:10.1016/j.solmat.2018.08.011.
26. Guldin, S.; Kohn, P.; Stefik, M.; Song, J.; Divitini, G.; Ecarla, F.; Ducati, C.; Wiesner, U.; Steiner, U. Self-Cleaning Antireflective Optical Coatings. *Nano Lett.* **2013**, *13*, 5329–5335, doi:10.1021/nl402832u.
27. Bellanger, H.; Darmanin, T.; Taffin de Givenchy, E.; Guittard, F. Chemical and Physical Pathways for the Preparation of Superoleophobic Surfaces and Related Wetting Theories. *Chem. Rev.* **2014**, *114*, 2694–2716, doi:10.1021/cr400169m.
28. Du, Y.; Lv, Y.; Wang, F.; Li, X.; Li, C. Effect of TiO2 Nanoparticles on the Breakdown Strength of Transformer Oil. In Proceedings of the 2010 IEEE International Symposium on Electrical Insulation; IEEE: San Diego, CA, USA, June 2010; pp. 1–3.
29. Hoffmann, M.R.; Martin, S.T.; Choi, Wonyong.; Bahnemann, D.W. Environmental Applications of Semiconductor Photocatalysis. *Chem. Rev.* **1995**, *95*, 69–96, doi:10.1021/cr00033a004.
30. Gupta, S.M.; Tripathi, M. A Review of TiO2 Nanoparticles. *Chin. Sci. Bull.* **2011**, *56*, 1639–1657, doi:10.1007/s11434-011-4476-1.
31. Enright, B.; Fitzmaurice, D. Spectroscopic Determination of Electron and Hole Effective Masses in a Nanocrystalline Semiconductor Film. *J. Phys. Chem.* **1996**, *100*, 1027–1035, doi:10.1021/jp951142w.
32. Pighini, C. Synthèses de nanocristaux de TiO2 anatase à distribution de taille contrôlée. Influence de la taille des cristallites sur le spectre Raman et étude des propriétés de surface. 207.
33. Zhang, L.D.; Zhang, H.F.; Wang, G.Z.; Mo, C.M.; Zhang, Y. Dielectric Behaviour of Nano-TiO2 Bulks. *Phys. Status Solidi A* **1996**, *157*, 483–491, doi:10.1002/pssa.2211570232.

34. Liu, G.; Jian, W.; Jin, H.; Shi, Z.; Qiao, G. A High Dielectric Constant in Nano-TiO2 Ceramic Prepared by a Rapid and High-Pressure Sintering Process. *Scr. Mater.* **2011**, *65*, 588–591, doi:10.1016/j.scriptamat.2011.06.031.
35. S., A.B.; S., C.V.; S., N.C.; P., R.M.; S., J.H.; Lamani, A.R. Influence of Particle Size on Band Gap and Dielectric Properties of TiO2 Nanomaterials.; Bikaner, India, 2016; p. 020347.
36. Davis, J.A. Energy Density Limits of Multiphase Composites With Dielectric Nanoparticles. *IEEE Trans. Nanotechnol.* **2018**, *17*, 250–260, doi:10.1109/TNANO.2018.2790955.
37. Dang, Z.-M.; Yuan, J.-K.; Yao, S.-H.; Liao, R.-J. Flexible Nanodielectric Materials with High Permittivity for Power Energy Storage. *Adv. Mater.* **2013**, *25*, 6334–6365, doi:10.1002/adma.201301752.
38. Sarkar, D.K.; Brassard, D.; El Khakani, M.A.; Ouellet, L. Single-Electron Tunneling at Room Temperature in TixSi1−xO2 Nanocomposite Thin Films. *Appl. Phys. Lett.* **2005**, *87*, 253108, doi:10.1063/1.2147729.
39. Fanelli, F.; Fracassi, F. Aerosol-Assisted Atmospheric Pressure Cold Plasma Deposition of Organic–Inorganic Nanocomposite Coatings. *Plasma Chem. Plasma Process.* **2014**, *34*, 473–487, doi:10.1007/s11090-013-9518-9.
40. Ajayan, P.M.; Schadler, L.S.; Braun, P.V. *Nanocomposite Science and Technology*; 2nd repr.; Wiley-VCH: Weinheim, 2005; ISBN 978-3-527-30359-5.
41. Kermadi, S.; Agoudjil, N.; Sali, S.; Boumaour, M.; Bourgeois, S.; Marco de Lucas, M.C. Sol-Gel Synthesis of XTiO2(100−x)SiO2 Nanocomposite Thin Films: Structure, Optical and Antireflection Properties. *Thin Solid Films* **2014**, *564*, 170–178, doi:10.1016/j.tsf.2014.05.068.
42. Kermadi, S.; Agoudjil, N.; Sali, S.; Zougar, L.; Boumaour, M.; Broch, L.; En Naciri, A.; Placido, F. Microstructure and Optical Dispersion Characterization of Nanocomposite Sol–Gel TiO 2 –SiO 2 Thin Films with Different Compositions. *Spectrochim. Acta. A. Mol. Biomol. Spectrosc.* **2015**, *145*, 145–154, doi:10.1016/j.saa.2015.02.110.
43. Lopes de Jesus, M.A.M.; de Magalhães Gomes, G.H.; Ferlauto, A.S.; Seara, L.M.; de Mello Ferreira, A.; Della Santina Mohallem, N. A Systematic Study of Multifunctional XTiO2/(100 − x)SiO2 Thin Films Prepared by Sol–Gel Process. *J. Sol-Gel Sci. Technol.* **2019**, *89*, 380–391, doi:10.1007/s10971-018-4867-8.
44. Charitidis, C.A.; Georgiou, P.; Koklioti, M.A.; Trompeta, A.-F.; Markakis, V. Manufacturing Nanomaterials: From Research to Industry. *Manuf. Rev.* **2014**, *1*, 11, doi:10.1051/mfreview/2014009.
45. Hench, L.L.; West, J.K. The Sol-Gel Process. *Chem. Rev.* **1990**, *90*, 33–72, doi:10.1021/cr00099a003.
46. Kwiatkowski, K.; Lukehart, C. Nanocomposites prepared by sol-gel methodsSynthesis and characterization. In *Handbook of Nanostructured Materials and Nanotechnology*; Elsevier, 2000; Vol. 1, pp. 387–421 ISBN 978-0-12-513760-7.
47. Nikam, A.V.; Prasad, B.L.V.; Kulkarni, A.A. Wet Chemical Synthesis of Metal Oxide Nanoparticles: A Review. *CrystEngComm* **2018**, *20*, 5091–5107, doi:10.1039/C8CE00487K.
48. *Sol-Gel Nanocomposites*; Guglielmi, M., Kickelbick, G., Martucci, A., Eds.; Springer New York: New York, NY, 2014; ISBN 978-1-4939-1208-7.
49. Ebelmen Sur l'hyalite artificielle et l'hydrophane. *Comptes Rendus Hebd. Séances Académie Sci.* **1847**, *25*, 854–856.
50. Dong, W.; Lee, C.W.; Lu, X.; Sun, Y.; Hua, W.; Zhuang, G.; Zhang, S.; Chen, J.; Hou, H.; Zhao, D. Synchronous Role of Coupled Adsorption and Photocatalytic Oxidation on Ordered Mesoporous Anatase TiO2–SiO2 Nanocomposites Generating Excellent Degradation Activity of RhB Dye. *Appl. Catal. B Environ.* **2010**, *95*, 197–207, doi:10.1016/j.apcatb.2009.12.025.

51. Nilchi, A.; Janitabar-Darzi, S.; Mahjoub, A.R.; Rasouli-Garmarodi, S. New TiO2/SiO2 Nanocomposites—Phase Transformations and Photocatalytic Studies. *Colloids Surf. Physicochem. Eng. Asp.* **2010**, *361*, 25–30, doi:10.1016/j.colsurfa.2010.03.006.
52. Nilchi, A.; Janitabar-Darzi, S.; Rasouli-Garmarodi, S. Sol-Gel Preparation of Nanoscale TiO₂/SiO₂ Composite for Eliminating of Con Red Azo Dye. *Mater. Sci. Appl.* **2011**, *02*, 476–480, doi:10.4236/msa.2011.25064.
53. Dong, W.; Sun, Y.; Ma, Q.; Zhu, L.; Hua, W.; Lu, X.; Zhuang, G.; Zhang, S.; Guo, Z.; Zhao, D. Excellent Photocatalytic Degradation Activities of Ordered Mesoporous Anatase TiO2–SiO2 Nanocomposites to Various Organic Contaminants. *J. Hazard. Mater.* **2012**, *229–230*, 307–320, doi:10.1016/j.jhazmat.2012.06.002.
54. Pinho, L.; Mosquera, M.J. Photocatalytic Activity of TiO2–SiO2 Nanocomposites Applied to Buildings: Influence of Particle Size and Loading. *Appl. Catal. B Environ.* **2013**, *134–135*, 205–221, doi:10.1016/j.apcatb.2013.01.021.
55. Mao, Q.; Zeng, D.; Xu, K.; Xie, C. Fabrication of Porous TiO_2 –SiO_2 Multifunctional Anti-Reflection Coatings by Sol–Gel Spin Coating Method. *RSC Adv* **2014**, *4*, 58101–58107, doi:10.1039/C4RA10424B.
56. Holtzinger, C.; Rapenne, L.; Chaudouët, P.; Berthomé, G.; Joud, J.C.; Langlet, M. Influence of Sol Composition on Natural Superhydrophilicity of Sol Gel–Derived TiO_2 –SiO_2 Nanocomposite Thin Films. *Emerg. Mater. Res.* **2012**, *1*, 127–135, doi:10.1680/emr.11.00024.
57. Pakdel, E.; Daoud, W.A.; Wang, X. Self-Cleaning and Superhydrophilic Wool by TiO2/SiO2 Nanocomposite. *Appl. Surf. Sci.* **2013**, *275*, 397–402, doi:10.1016/j.apsusc.2012.10.141.
58. de Chiara, M.L.V.; Pal, S.; Licciulli, A.; Amodio, M.L.; Colelli, G. Photocatalytic Degradation of Ethylene on Mesoporous TiO2/SiO2 Nanocomposites: Effects on the Ripening of Mature Green Tomatoes. *Biosyst. Eng.* **2015**, *132*, 61–70, doi:10.1016/j.biosystemseng.2015.02.008.
59. Kudryavtsev, P.G.; Figovsky, O.L. NANOCOMPOSITES BASED ON HYBRID ORGANO-SILICATE MATRIX. **2016**, 23.
60. Kondratiev, V. Processing and Characterization of Transparent Electrode Materials. **2017**, doi:10.13140/RG.2.2.34906.24008.
61. Chen, C.; Bai, H.; Chein, H.; Chen, T.M. Continuous Generation of TiO_2 Nanoparticles by an Atmospheric Pressure Plasma-Enhanced Process. *Aerosol Sci. Technol.* **2007**, *41*, 1018–1028, doi:10.1080/02786820701694355.
62. Chen, C.; Bai, H.; Chang, C. Effect of Plasma Processing Gas Composition on the Nitrogen-Doping Status and Visible Light Photocatalysis of TiO_2. *J. Phys. Chem. C* **2007**, *111*, 15228–15235, doi:10.1021/jp0716233.
63. Liu, W.-J.; Lai, Y.-L. Investigation of Novel Low Temperature Atmospheric Pressure Plasma System for Deposition Photo-Catalytic TiO2 Thin Film. *Surf. Modif. Mater. Ion Beams 2009* **2011**, *206*, 959–962, doi:10.1016/j.surfcoat.2011.03.103.
64. Klenko, Y.; Pichal, J. TiOx Films Deposited by Plasma Enhanced Chemical Vapour Deposition Method in Atmospheric Dielectric Barrier Discharge Plasma. *Plasma Chem. Plasma Process.* **2012**, *32*, 1215–1225, doi:10.1007/s11090-012-9401-0.
65. Shirafuji, T.; Miyazaki, Y.; Hayashi, Y.; Nishino, S. PE-CVD of Fluorocarbon/SiO Composite Thin Films Using C4F8 and HMDSO. *Plasmas Polym.* **1999**, *4*, 57–75, doi:10.1023/A:1021803615715.
66. Choukourov, A.; Pihosh, Y.; Stelmashuk, V.; Biederman, H.; Slavínská, D.; Kormunda, M.; Zajíčková, L. Rf Sputtering of Composite SiOx/Plasma Polymer Films and Their Basic Properties. *Proc. Symp. C Prtoective Coat. Thin Films* **2002**, *151–152*, 214–217, doi:10.1016/S0257-8972(01)01622-X.
67. Granier, A.; Borvon, G.; Bousquet, A.; Goullet, A.; Leteinturier, C.; van der Lee, A. Mechanisms Involved in the Conversion of PpHMDSO Films into SiO2-Like by Oxygen Plasma Treatment. *Plasma Process. Polym.* **2006**, *3*, 365–373, doi:10.1002/ppap.200600022.

68. Drabik, M.; Kousal, J.; Pihosh, Y.; Choukourov, A.; Biederman, H.; Slavinska, D.; Mackova, A.; Boldyreva, A.; Pesicka, J. Composite SiOx/Hydrocarbon Plasma Polymer Films Prepared by RF Magnetron Sputtering of SiO2 and Polyimide. *Vacuum* **2007**, *81*, 920–927, doi:10.1016/j.vacuum.2006.10.013.
69. Bousquet, A.; Goullet, A.; Leteinturier, C.; Coulon, N.; Granier, A. Influence of Ion Bombardment on Structural and Electrical Properties of SiO_2 Thin Films Deposited from O_2/HMDSO Inductively Coupled Plasmas under Continuous Wave and Pulsed Modes. *Eur. Phys. J. Appl. Phys.* **2008**, *42*, 3–8, doi:10.1051/epjap:2008038.
70. Hu, E.-T.; Liu, X.-X.; Cai, Q.-Y.; Yao, Y.; Zang, K.-Y.; Yu, K.-H.; Wei, W.; Xu, X.-X.; Zheng, Y.-X.; Wang, S.-Y.; et al. Tunable Optical Properties of Co-Sputtered Ti-SiO_2 Nanocomposite Thin Films. *Opt. Mater. Express* **2017**, *7*, 2387, doi:10.1364/OME.7.002387.
71. Chen, J.-S.; Chao, S.; Kao, J.-S.; Niu, H.; Chen, C.-H. Mixed Films of TiO_2–SiO_2 Deposited by Double Electron-Beam Coevaporation. *Appl. Opt.* **1996**, *35*, 90, doi:10.1364/AO.35.000090.
72. Ghodselahi, T.; Vesaghi, M.A.; Shafiekhani, A.; Baradaran, A.; Karimi, A.; Mobini, Z. Co-Deposition Process of RF-Sputtering and RF-PECVD of Copper/Carbon Nanocomposite Films. *Surf. Coat. Technol.* **2008**, *202*, 2731–2736, doi:10.1016/j.surfcoat.2007.10.009.
73. El Mel, A.A.; Angleraud, B.; Gautron, E.; Granier, A.; Tessier, P.Y. Microstructure and Composition of TiC/a-C:H Nanocomposite Thin Films Deposited by a Hybrid IPVD/PECVD Process. *Surf. Coat. Technol.* **2010**, *204*, 1880–1883, doi:10.1016/j.surfcoat.2009.09.045.
74. Kolipaka, K.L.; Brueser, V.; Schlueter, R.; Quade, A.; Schaefer, J.; Wulff, H.; Strunskus, T.; Faupel, F. Simple Method of Hybrid PVD/PECVD to Prepare Well-Dispersed Cobalt–Plasma Polymerized Hexamethyldisilazane Nanocomposites. *Surf. Coat. Technol.* **2012**, *207*, 565–570, doi:10.1016/j.surfcoat.2012.07.073.
75. Bedel, L.; Cayron, C.; Jouve, M.; Maury, F. Embedded Layer of Ag Nanoparticles Prepared by a Combined PECVD/PVD Process Producing $SiO_x C_y$–Ag Nanocomposite Thin Films. *Nanotechnology* **2012**, *23*, 015603, doi:10.1088/0957-4484/23/1/015603.
76. Kylián, O.; Štefaníková, R.; Kuzminova, A.; Hanuš, J.; Solař, P.; Kúš, P.; Cieslar, M.; Biederman, H. In-Flight Plasma Modification of Nanoparticles Produced by Means of Gas Aggregation Sources as an Effective Route for the Synthesis of Core-Satellite Ag/Plasma Polymer Nanoparticles. *Plasma Phys. Control. Fusion* **2020**, *62*, 014005, doi:10.1088/1361-6587/ab4115.
77. Biederman, H.; Kylian, O.; Drabik, M.; Choukourov, A.; Polonskyi, O.; Solar, P. Nanocomposite and Nanostructured Films with Plasma Polymer Matrix. *Surf. Coat. Technol.* **2012**, *211*, 127–137, doi:10.1016/j.surfcoat.2011.09.011.
78. Biederman, H. Nanocomposites and Nanostructures Based on Plasma Polymers. *Surf. Coat. Technol.* **2011**, *205*, S10–S14, doi:10.1016/j.surfcoat.2011.03.115.
79. Patelli, N.; Migliori, A.; Morandi, V.; Pasquini, L. One-Step Synthesis of Metal/Oxide Nanocomposites by Gas Phase Condensation. *Nanomaterials* **2019**, *9*, 219, doi:10.3390/nano9020219.
80. Nikitin, D.; Hanuš, J.; Ali-Ogly, S.; Polonskyi, O.; Drewes, J.; Faupel, F.; Biederman, H.; Choukourov, A. The Evolution of Ag Nanoparticles inside a Gas Aggregation Cluster Source. *Plasma Process. Polym.* **2019**, *16*, 1900079, doi:10.1002/ppap.201900079.
81. Košutová, T.; Horák, L.; Shelemin, A.; Vaidulych, M.; Hanuš, J.; Biederman, H.; Kylián, O.; Solař, P.; Cieslar, M.; Choukourov, A.; et al. Synthesis and Microstructure Investigation of Heterogeneous Metal-Plasma Polymer Ag/HMDSO Nanoparticles. *Surf. Interface Anal.* **2020**, doi:10.1002/sia.6779.
82. Solař, P.; Hanuš, J.; Cieslar, M.; Košutová, T.; Škorvánková, K.; Kylián, O.; Kúš, P.; Biederman, H. Composite Ni@Ti Nanoparticles Produced in Arrow-Shaped Gas Aggregation Source. *J. Phys. Appl. Phys.* **2020**, *53*, 195303, doi:10.1088/1361-6463/ab7353.

83. Balasubramanian, B.; Kraemer, K.L.; Reding, N.A.; Skomski, R.; Ducharme, S.; Sellmyer, D.J. Synthesis of Monodisperse TiO2−Paraffin Core−Shell Nanoparticles for Improved Dielectric Properties. *ACS Nano* **2010**, *4*, 1893–1900, doi:10.1021/nn9016422.
84. Drabik, M.; Choukourov, A.; Artemenko, A.; Polonskyi, O.; Kylian, O.; Kousal, J.; Nichtova, L.; Cimrova, V.; Slavinska, D.; Biederman, H. Structure and Composition of Titanium Nanocluster Films Prepared by a Gas Aggregation Cluster Source. *J. Phys. Chem. C* **2011**, *115*, 20937–20944, doi:10.1021/jp2059485.
85. Martínez, L.; Mayoral, A.; Espiñeira, M.; Roman, E.; Palomares, F.J.; Huttel, Y. Core@shell, Au@TiOx Nanoparticles by Gas Phase Synthesis. *Nanoscale* **2017**, *9*, 6463–6470, doi:10.1039/C7NR01148B.
86. Kousal, J.; Kolpaková, A.; Shelemin, A.; Kudrna, P.; Tichý, M.; Kylián, O.; Hanuš, J.; Choukourov, A.; Biederman, H. Monitoring of Conditions inside Gas Aggregation Cluster Source during Production of Ti/TiOxnanoparticles. *Plasma Sources Sci. Technol.* **2017**, *26*, 105003, doi:10.1088/1361-6595/aa88e8.
87. *Gas-Phase Synthesis of Nanoparticles*; Huttel, Y., Ed.; Wiley-VCH: Weinheim, Germany, 2017; ISBN 978-3-527-34060-6.
88. Kratochvíl, J.; Kuzminova, A.; Kylián, O. State-of-the-Art, and Perspectives of, Silver/Plasma Polymer Antibacterial Nanocomposites. *Antibiotics* **2018**, *7*, 78, doi:10.3390/antibiotics7030078.
89. Nandiyanto, A.B.D.; Okuyama, K. Progress in Developing Spray-Drying Methods for the Production of Controlled Morphology Particles: From the Nanometer to Submicrometer Size Ranges. *Adv. Powder Technol.* **2011**, *22*, 1–19, doi:10.1016/j.apt.2010.09.011.
90. Suhendi, A.; Nandiyanto, A.B.D.; Munir, M.M.; Ogi, T.; Gradon, L.; Okuyama, K. Self-Assembly of Colloidal Nanoparticles Inside Charged Droplets during Spray-Drying in the Fabrication of Nanostructured Particles. *Langmuir* **2013**, *29*, 13152–13161, doi:10.1021/la403127e.
91. Wang, X.; Masumoto, H.; Someno, Y.; Hirai, T. Microstructure and Optical Properties of Amorphous TiO2-SiO2 Composite ®lms Synthesized by Helicon Plasma Sputtering. *Thin Solid Films* **1999**, 5.
92. Wang, W.-N.; Itoh, Y.; Lenggoro, I.W.; Okuyama, K. Nickel and Nickel Oxide Nanoparticles Prepared from Nickel Nitrate Hexahydrate by a Low Pressure Spray Pyrolysis. *Mater. Sci. Eng. B* **2004**, *111*, 69–76, doi:10.1016/j.mseb.2004.03.024.
93. Wang, W.-N.; Purwanto, A.; Lenggoro, I.W.; Okuyama, K.; Chang, H.; Jang, H.D. Investigation on the Correlations between Droplet and Particle Size Distribution in Ultrasonic Spray Pyrolysis. *Ind. Eng. Chem. Res.* **2008**, *47*, 1650–1659, doi:10.1021/ie070821d.
94. Schaldach, G.; Berger, L.; Razilov, I.; Berndt, H. Characterization of a Cyclone Spray Chamber for ICP Spectrometry by Computer Simulation. *J. Anal. At. Spectrom.* **2002**, *17*, 334–344, doi:10.1039/b106024b.
95. Westphal, C.S.; Kahen, K.; Rutkowski, W.F.; Acon, B.W.; Montaser, A. Demountable Direct Injection High Efficiency Nebulizer for Inductively Coupled Plasma Mass Spectrometry. *Spectrochim. Acta Part B At. Spectrosc.* **2004**, *59*, 353–368, doi:10.1016/j.sab.2004.01.004.
96. Matusiewicz, H.; Ślachciński, M. Simultaneous Determination of As, Bi, Sb, Se and Sn by Microwave Induced Plasma Spectrometry Using a Quadruple-Mode Microflow Ultrasonic Nebulizer for in Situ Hydride Generation with Internal Standardization. *Microchem. J.* **2017**, *131*, 70–78, doi:10.1016/j.microc.2016.11.017.
97. Giersz, J.; Bartosiak, M.; Jankowski, K. Sensitive Determination of Hg Together with Mn, Fe, Cu by Combined Photochemical Vapor Generation and Pneumatic Nebulization in the Programmable Temperature Spray Chamber and Inductively Coupled Plasma Optical Emission Spectrometry. *Talanta* **2017**, *167*, 279–285, doi:10.1016/j.talanta.2017.02.018.

98. Matusiewicz, H.; Ślachciński, M. Analytical Evaluation of a Quadruple-Mode Micro-Flow Ultrasonic Nebulizer for Sample Introduction in Microwave Induced Plasma Spectrometry. *Microchem. J.* **2017**, *130*, 345–352, doi:10.1016/j.microc.2016.10.010.
99. Brinley, E.; Babu, K.S.; Seal, S. The Solution Precursor Plasma Spray Processing of Nanomaterials. *JOM* **2007**, *59*, 54–59, doi:10.1007/s11837-007-0090-8.
100. Boscher, N.D.; Choquet, P.; Duday, D.; Kerbellec, N.; Lambrechts, J.-C.; Maurau, R. Luminescent Lanthanide-Based Hybrid Coatings Deposited by Atmospheric Pressure Plasma Assisted Chemical Vapour Deposition. *J. Mater. Chem.* **2011**, *21*, 18959, doi:10.1039/c1jm14659a.
101. Fauchais, P.; Joulia, A.; Goutier, S.; Chazelas, C.; Vardelle, M.; Vardelle, A.; Rossignol, S. Suspension and Solution Plasma Spraying. *J. Phys. Appl. Phys.* **2013**, *46*, 224015, doi:10.1088/0022-3727/46/22/224015.
102. Haapanen, J.; Aromaa, M.; Teisala, H.; Tuominen, M.; Stepien, M.; Saarinen, J.J.; Heikkilä, M.; Toivakka, M.; Kuusipalo, J.; Mäkelä, J.M. Binary TiO2/SiO2 Nanoparticle Coating for Controlling the Wetting Properties of Paperboard. *Mater. Chem. Phys.* **2015**, *149–150*, 230–237, doi:10.1016/j.matchemphys.2014.10.011.
103. Dembele, A.; Rahman, M.; Reid, I.; Twomey, B.; MacElroy, J.M.D.; Dowling, D.P. Deposition of Hybrid Organic–Inorganic Composite Coatings Using an Atmospheric Plasma Jet System. *J. Nanosci. Nanotechnol.* **2011**, *11*, 8730–8737, doi:10.1166/jnn.2011.3459.
104. Schäfer, J.; Fricke, K.; Mika, F.; Pokorná, Z.; Zajíčková, L.; Foest, R. Liquid Assisted Plasma Enhanced Chemical Vapour Deposition with a Non-Thermal Plasma Jet at Atmospheric Pressure. *Thin Solid Films* **2017**, *630*, 71–78, doi:10.1016/j.tsf.2016.09.022.
105. Liguori, A.; Traldi, E.; Toccaceli, E.; Laurita, R.; Pollicino, A.; Focarete, M.L.; Colombo, V.; Gherardi, M. Co-Deposition of Plasma-Polymerized Polyacrylic Acid and Silver Nanoparticles for the Production of Nanocomposite Coatings Using a Non-Equilibrium Atmospheric Pressure Plasma Jet: Co-Deposition of Plasma-Polymerized Polyacrylic Acid and Silver Nanoparticles…. *Plasma Process. Polym.* **2016**, *13*, 623–632, doi:10.1002/ppap.201500143.
106. Marino, E.; Huijser, T.; Creyghton, Y.; van der Heijden, A. Synthesis and Coating of Copper Oxide Nanoparticles Using Atmospheric Pressure Plasmas. *Surf. Coat. Technol.* **2007**, *201*, 9205–9208, doi:10.1016/j.surfcoat.2007.04.091.
107. Bardon, J.; Bour, J.; Del Frari, D.; Arnoult, C.; Ruch, D. Dispersion of Cerium-Based Nanoparticles in an Organosilicon Plasma Polymerized Coating: Effect on Corrosion Protection. *Plasma Process. Polym.* **2009**, *6*, S655–S659, doi:10.1002/ppap.200931710.
108. Del Frari, D.; Bour, J.; Bardon, J.; Buchheit, O.; Arnoult, C.; Ruch, D. Hybrid Layers Deposited by an Atmospheric Pressure Plasma Process for Corrosion Protection of Galvanized Steel. *J. Nanosci. Nanotechnol.* **2010**, *10*, 2611–2619, doi:10.1166/jnn.2010.1460.
109. Fanelli, F.; Mastrangelo, A.M.; Fracassi, F. Aerosol-Assisted Atmospheric Cold Plasma Deposition and Characterization of Superhydrophobic Organic–Inorganic Nanocomposite Thin Films. *Langmuir* **2014**, *30*, 857–865, doi:10.1021/la404755n.
110. Profili, J.; Levasseur, O.; Blaisot, J.-B.; Koronai, A.; Stafford, L.; Gherardi, N. Nebulization of Nanocolloidal Suspensions for the Growth of Nanocomposite Coatings in Dielectric Barrier Discharges. *Plasma Process. Polym.* **2016**, *13*, 981–989, doi:10.1002/ppap.201500223.
111. Profili, J.; Levasseur, O.; Naudé, N.; Chaneac, C.; Stafford, L.; Gherardi, N. Influence of the Voltage Waveform during Nanocomposite Layer Deposition by Aerosol-Assisted Atmospheric Pressure Townsend Discharge. *J. Appl. Phys.* **2016**, *120*, 053302, doi:10.1063/1.4959994.
112. Profili, J.; Levasseur, O.; Koronai, A.; Stafford, L.; Gherardi, N. Deposition of Nanocomposite Coatings on Wood Using Cold Discharges at Atmospheric Pressure. *Surf. Coat. Technol.* **2017**, *309*, 729–737, doi:10.1016/j.surfcoat.2016.10.095.

113. Profili, J.; Dap, S.; Levasseur, O.; Naude, N.; Belinger, A.; Stafford, L.; Gherardi, N. Interaction of Atomized Colloid with an Ac Electric Field in a Dielectric Barrier Discharge Reactor Used for Deposition of Nanocomposite Coatings. *J. Phys. Appl. Phys.* **2017**, *50*, 075201, doi:10.1088/1361-6463/aa515f.
114. Brunet, P.; Rincón, R.; Martinez, J.-M.; Matouk, Z.; Fanelli, F.; Chaker, M.; Massines, F. Control of Composite Thin Film Made in an Ar/Isopropanol/TiO2 Nanoparticles Dielectric Barrier Discharge by the Excitation Frequency. *Plasma Process. Polym.* **2017**, doi:10.1002/ppap.201700049.
115. Brunet, P. Procédé de dépôt de couches minces nanocomposites par décharge à barrière diélectrique : de l'aérosol d'une suspension colloïdale à la morphologie du dépôt. 187.
116. Model 3076 Constant Output Atomizer Instruction Manual. 63.
117. Bruggeman, P.J.; Kushner, M.J.; Locke, B.R.; Gardeniers, J.G.E.; Graham, W.G.; Graves, D.B.; Hofman-Caris, R.C.H.M.; Maric, D.; Reid, J.P.; Ceriani, E.; et al. Plasma–Liquid Interactions: A Review and Roadmap. *Plasma Sources Sci. Technol.* **2016**, *25*, 053002, doi:10.1088/0963-0252/25/5/053002.
118. Hemmer, E.; Kumakiri, I.; Lecerf, N.; Bredesen, R.; Barth, S.; Altmayer, J.; Donia, N.; Cavelius, C.; Soga, K.; Mathur, S. Nanostructured ZrO2 Membranes Prepared by Liquid-Injection Chemical Vapor Deposition. *Microporous Mesoporous Mater.* **2012**, *163*, 229–236, doi:10.1016/j.micromeso.2012.06.057.
119. Avril, L.; Boudon, J.; Marco de Lucas, M.C.; Imhoff, L. Alumina Particle Reinforced TiO2 Composite Films Grown by Direct Liquid Injection MOCVD. *Vacuum* **2014**, *107*, 259–263, doi:10.1016/j.vacuum.2014.02.020.
120. Vervaele, M.; De Roo, B.; Deschaume, O.; Rajala, M.; Guillon, H.; Sousa, M.; Bartic, C.; Van Haesendonck, C.; Seo, J.W.; Locquet, J.-P. Development of a New Direct Liquid Injection System for Nanoparticle Deposition by Chemical Vapor Deposition Using Nanoparticle Solutions. *Rev. Sci. Instrum.* **2016**, *87*, 025101, doi:10.1063/1.4940937.
121. Li, Z.; Gordon, R.G.; Pallem, V.; Li, H.; Shenai, D.V. Direct-Liquid-Injection Chemical Vapor Deposition of Nickel Nitride Films and Their Reduction to Nickel Films. *Chem. Mater.* **2010**, *22*, 3060–3066, doi:10.1021/cm903636j.
122. Vervaele, M.; De Roo, B.; Debehets, J.; Sousa, M.; Zhang, L.; Van Bilzen, B.; Seré, S.; Guillon, H.; Rajala, M.; Seo, J.W.; et al. A Novel Direct Liquid Injection Low Pressure Chemical Vapor Deposition System (DLI-LPCVD) for the Deposition of Thin Films: A Novel Direct Liquid Injection Low Pressure Chemical…. *Adv. Eng. Mater.* **2017**, *19*, 1700193, doi:10.1002/adem.201700193.
123. Vervaele, M.; De Roo, B.; Debehets, J.; Sousa, M.; Zhang, L.; Van Bilzen, B.; Seré, S.; Guillon, H.; Rajala, M.; Won Seo, J.; et al. Direct Liquid Injection − Low Pressure Chemical Vapor Deposition of Silica Thin Films from Di-t-Butoxydiacetoxysilane. *Adv. Eng. Mater.* **2017**, 1700425, doi:10.1002/adem.201700425.
124. Avril, L.; Decams, J.M.; Imhoff, L. Pulsed Direct Liquid Injection ALD of TiO2 Films Using Titanium Tetraisopropoxide Precursor. *Phys. Procedia* **2013**, *46*, 33–39, doi:10.1016/j.phpro.2013.07.063.
125. Avril, L.; Reymond-Laruinaz, S.; Decams, J.M.; Bruyère, S.; Potin, V.; de Lucas, M.C.M.; Imhoff, L. TiO2 Anatase Films Obtained by Direct Liquid Injection Atomic Layer Deposition at Low Temperature. *Appl. Surf. Sci.* **2014**, *288*, 201–207, doi:10.1016/j.apsusc.2013.10.007.
126. Ross, A.D.; Gleason, K.K. The CVD of Nanocomposites Fabricated via Ultrasonic Atomization. *Chem. Vap. Depos.* **2006**, *12*, 225–230, doi:10.1002/cvde.200506368.
127. Ogawa, D.; Saraf, I.; Sra, A.; Timmons, R.; Goeckner, M.; Overzet, L. The Direct Injection of Liquid Droplets into Low Pressure Plasmas. *J. Vac. Sci. Technol. Vac. Surf. Films* **2009**, *27*, 342–351, doi:10.1116/1.3081965.

128. Ogawa, D.; Chung, C.W.; Goeckner, M.; Overzet, L. Transient Effects Caused by Pulsed Gas and Liquid Injections into Low Pressure Plasmas. *Plasma Sources Sci. Technol.* **2010**, *19*, 034013, doi:10.1088/0963-0252/19/3/034013.
129. Goeckner, M.; Ogawa, D.; Saraf, I.; Overzet, L. Progress Report: Direct Injection of Liquids into Low-Pressure Plasmas. *J. Phys. Conf. Ser.* **2009**, *162*, 012014, doi:10.1088/1742-6596/162/1/012014.
130. Coppins, M. The Critical Droplet Size in a Misty Plasma. 4.
131. Coppins, M. Electrostatic Breakup in a Misty Plasma. *Phys. Rev. Lett.* **2010**, *104*, doi:10.1103/PhysRevLett.104.065003.
132. Carnide, G. Procédé de Dépôt Couplant Un Réacteur-Injecteur et Un Plasma Basse Pression - Vers Le Dépôt de Couches Minces Multifonctionnelles Pour l'aéronautique, Toulouse 3: Toulouse, France, 2020.
133. Kahn, M.; Champouret, Y.; Clergereaux, R.; Vahlas, C.; Mingotaud, A.-F.; Carnide, G. Procédé de Préparation de Nanoparticules.
134. Mitronika, M.; Profili, J.; Goullet, A.; Gautier, N.; Stephant, N.; Stafford, L.; Granier, A.; Richard-Plouet, M. TiO2–SiO2 Nanocomposite Thin Films Deposited by Direct Liquid Injection of Colloidal Solution in an O2/HMDSO Low-Pressure Plasma. *Appl Phys* **2021**, 14.
135. Karpinski, A. Couches Interfaciales TiO2 et NiO Déposées Pas CSD et PVD, Pour Cellules Solaires Organiques, Université de Nantes: Université de Nantes, 2011.
136. Karpinski, A.; Berson, S.; Terrisse, H.; Mancini-Le Granvalet, M.; Guillerez, S.; Brohan, L.; Richard-Plouet, M. Anatase Colloidal Solutions Suitable for Inkjet Printing: Enhancing Lifetime of Hybrid Organic Solar Cells. *Sol. Energy Mater. Sol. Cells* **2013**, *116*, 27–33, doi:10.1016/j.solmat.2013.04.006.
137. Brust, M.; Walker, M.; Bethell, D.; Schiffrin, D.J.; Whyman, R. Synthesis of Thiol-Derivatised Gold Nanoparticles in a Two-Phase Liquid–Liquid System. *J Chem Soc Chem Commun* **1994**, *0*, 801–802, doi:10.1039/C39940000801.
138. Karpinski, A.; Berson, S.; Terrisse, H.; Mancini-Le Granvalet, M.; Guillerez, S.; Brohan, L.; Richard-Plouet, M. Anatase Colloidal Solutions Suitable for Inkjet Printing: Enhancing Lifetime of Hybrid Organic Solar Cells. *Sol. Energy Mater. Sol. Cells* **2013**, *116*, 27–33, doi:10.1016/j.solmat.2013.04.006.
139. El Kass, M.; Brohan, L.; Gautier, N.; Béchu, S.; David, C.; Lemaitre, N.; Berson, S.; Richard-Plouet, M. TiO_2 Anatase Solutions for Electron Transporting Layers in Organic Photovoltaic Cells. *ChemPhysChem* **2017**, *18*, 2390–2396, doi:10.1002/cphc.201700306.
140. Mitronika, M.; Profili, J.; Goullet, A.; Stafford, L.; Granier, A.; Richard-Plouet, M. Modification of the Optical Properties and Nano-Crystallinity of Anatase TiO2nanoparticles Thin Film Using Low Pressure O2 Plasma Treatment. *Thin Solid Films* **2020**, *709*, 138212, doi:10.1016/j.tsf.2020.138212.